Chem

CellPress
REVIEWS

Review

Direct Methane Conversion under Mild Condition by Thermo-, Electro-, or Photocatalysis

Xianguang Meng,[1] Xiaoju Cui,[1,2,3] N. Pethan Rajan,[1] Liang Yu,[1,3] Dehui Deng,[1,2,3,*] and Xinhe Bao[1,3]

Direct conversion of earth-abundant methane into value-added chemicals under mild conditions is an attractive technology in response to the increasing industrial demand of feedstocks and worldwide appeal of energy conservation. Exploring advanced low-temperature C–H activation catalysts and reaction systems is the key to converting methane in a direct and mild manner. The recently developed reaction processes operated at low-temperature thermocatalysis systems or driven in electro- and photocatalysis systems shine light on the way to achieve efficient methane conversion with much economical energy input. In this review, we summarize the typical catalytic processes employed in these reaction systems and in particular highlight the potential heterogeneous catalysts with noteworthy C–H activation performance. We also present the progress along with our perspectives on catalyst design, theoretical simulations, the choice of reaction condition, and the method of reaction product analysis to encourage more viable technology for low-temperature methane conversion in the future.

INTRODUCTION

Methane is one of the most important fossil fuels and widely distributed in natural gas, shale gas, coalbed gas, combustible ice, biogas, etc. It is not only a source of clean energy widely used today but also a C1 building block for producing chemicals. Since methane is abundant and inexpensive, production of chemicals from methane has aroused intense interest from both academic and industrial communities. The methane molecule is in the form of a regular tetrahedron, and this stable non-polar structure leads to low polarizability and extremely high dissociation energy of its C–H bond (439.3 kJ mol^{-1}) (Figure 1). High reaction temperature in a wide range of methane conversions is needed for the tough process of C–H bond activation. Therefore, the methane conversion has been regarded as the ''holy grail'' in catalysis. In the conventional process that has been industrially implemented, methane is indirectly converted into liquid hydrocarbons in large scale through steam-methane reforming and Fischer-Tropsch (FT) synthesis. Steam-methane reforming for the production of syngas (a mixture of CO and H_2 as the feedstock of FT synthesis) is very endothermic (ΔH^0_{298K} = +206.2 kJ mol^{-1}), which makes the reaction process highly energy intensive. The reaction is normally operated at high temperature (700°C–1100°C) over an alumina-supported nickel catalyst. Since a huge amount of heat must be supplied in the syngas-based route, the direct routes of methane to chemicals at low temperature without going through the intermediate syngas production step has attracted great attention in the recent years. Some well-known direct methane conversion reactions include partial oxidation of methane (POM), oxidative coupling of methane (OCM), methane conversion to olefins, and aromatics in a

The Bigger Picture

Direct low-temperature methane conversion is a promising route for the chemical industry to access various basic feedstocks in the future. Developing such technology to displace the traditional energy-intensive syngas pathway has attracted increasing interest. A key for this technology is to seek advanced catalytic systems that enable efficient C–H activation along with a controllable reaction kinetics process. Therefore, it is important to take advantage of the various types of catalytic materials to effectively transform thermal, electric, and photonic energies into the driving forces for C–H activation. In this review, we present recent experimental and theoretical progress in the design of direct low-temperature methane conversion catalysts as well as the C–H activation mechanism in thermocatalysis, electrocatalysis, and photocatalysis systems to encourage more viable technologies for this challenging subject.

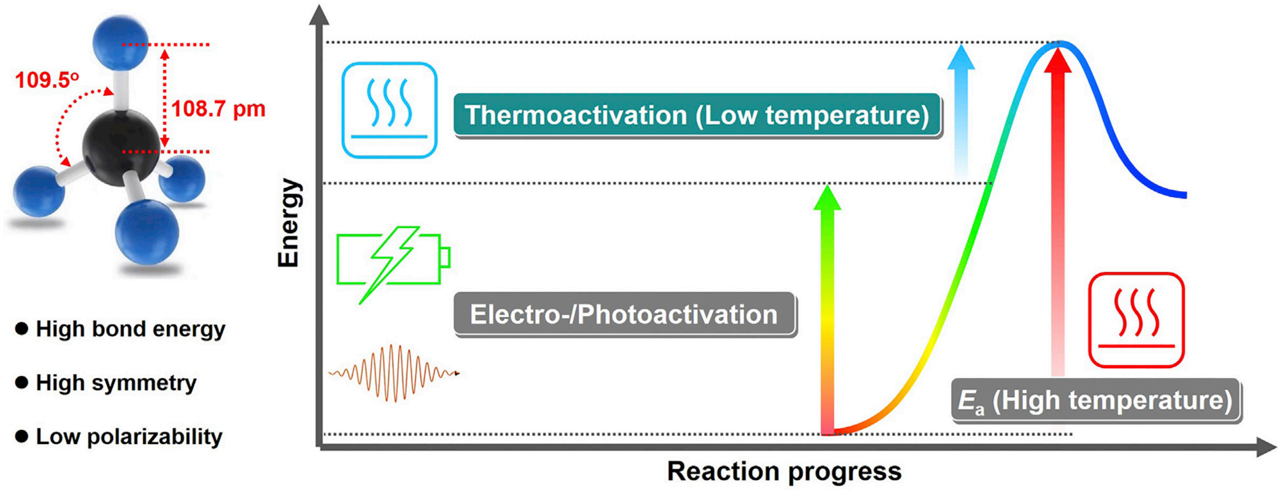

Figure 1. The Molecular Structure of Methane (Left) and Schematic Illustration of an Energy Diagram for Low-Temperature Methane Activation in Electro- and Photoactivation-Involved Reaction Systems (Right)

non-oxidative route, while their industrial applications are still hindered by the harsh reaction conditions (relatively high temperature and pressure), low yield, and low stability issues, etc.[1] The efficacy of catalysts for C–H activation plays a key role in displacing the energy-intensive syngas route by direct methane conversion. As a non-syngas-based route to transform methane into high-value-added chemicals, we have reported that the single iron sites embedded in a silica matrix enable direct, non-oxidative conversion of methane, exclusively to ethylene and aromatics.[2]

With the urgent need to reduce the cost from energy consumption and plant maintenance, direct methane conversion into (oxygenated) hydrocarbon products at low temperatures (<200°C) is very attractive, more economical, and environmentally friendly. Because oxidants are involved, the POM reactions become thermodynamically favorable at low temperatures and receive widespread attention. Formation of oxygenated products from POM, such as methanol being of great interest (Equation 1), is exothermic and much more simplified than the indirect syngas route. Such a favorable process, however, has not yet translated into industrial practice. Like the other methane conversion processes, POM also starts with the cleavage of C–H bond, and thus the catalysts should have good performance for C–H activation. Moreover, once the C–H bond of methane is activated, its oxygenated products are hard to be preserved in the general reaction conditions because the over-oxidation of these products into CO or CO_2 is thermodynamically more favorable (Equations 2, 3, and 4).[3,4] The over-oxidation is also promoted by the polar nature of oxygenated products, which are preferentially adsorbed on the catalysts for deep oxidation. Therefore, the key of direct methane conversion under mild conditions is to seek efficient low-temperature C–H activation catalysts and controllably mediate methane oxidation for selective oxygenated product formation.

$$CH_4 + 1/2O_2 = CH_3OH_{(g)}\ (\Delta H^0_{298K} = -126.4\ \text{kJ mol}^{-1}) \qquad \text{(Equation 1)}$$

$$CH_4 + O_2 = HCHO_{(g)} + H_2O(g)\ (\Delta H^0_{298K} = -276\ \text{kJ mol}^{-1}) \qquad \text{(Equation 2)}$$

$$CH_4 + 3/2O_2 = CO + 2H_2O(g)\ (\Delta H^0_{298K} = -519.6\ \text{kJ mol}^{-1}) \qquad \text{(Equation 3)}$$

$$CH_4 + 2O_2 = CO_2 + 2H_2O(g)\ (\Delta H^0_{298K} = -802.6\ \text{kJ mol}^{-1}) \qquad \text{(Equation 4)}$$

[1] State Key Laboratory of Catalysis, Collaborative Innovation Center of Chemistry for Energy Materials, Dalian Institute of Chemical Physics, Chinese Academy of Sciences, Dalian 116023, China

[2] State Key Laboratory of Physical Chemistry of Solid Surfaces, Collaborative Innovation Center of Chemistry for Energy Materials, College of Chemistry and Chemical Engineering, Xiamen University, Xiamen 361005, China

[3] University of Chinese Academy of Sciences, Beijing 100039, China

*Correspondence: dhdeng@dicp.ac.cn

https://doi.org/10.1016/j.chempr.2019.05.008

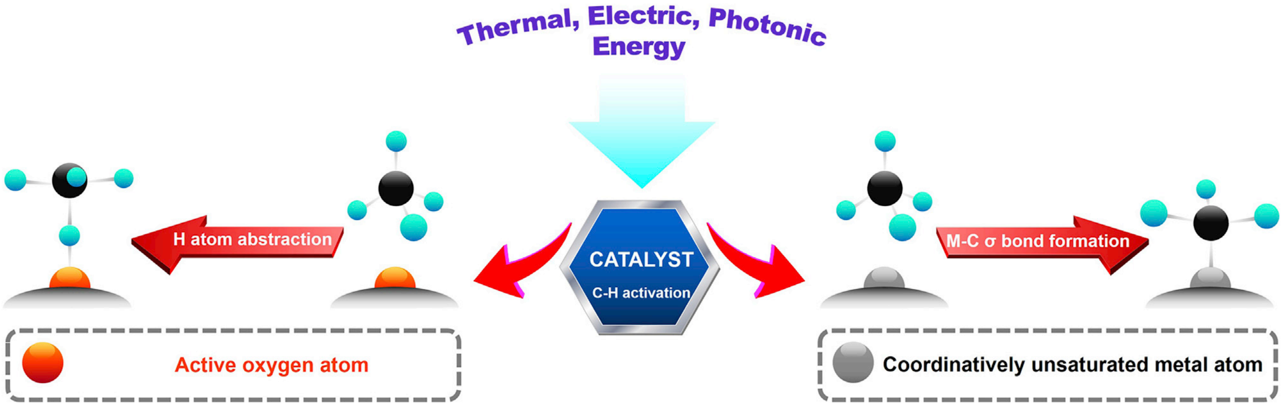

Figure 2. The Mechanism of C–H Bond Cleavage of Methane at Low-Temperature Reaction Systems

In most cases, direct POM by oxygen in a heterogeneous thermocatalysis system should be operated above 600°C.[5] With the aid of proper oxidants, such as H_2O_2, O_3, NO_x, $K_2S_2O_8$, and oleum, thermocatalytic POM can proceed at a much lower temperature. When external electric potentials or light irradiation is input as driving forces, the energy of electrons in catalytic reactions can be changed by several eV (around 3 eV), which is generally large enough to overcome the barriers of key intermediate steps related to C–H activation and realizes methane conversion at low temperature (Figure 1). Compared with thermocatalytic methane conversion, electrocatalytic methane conversion can be operated at more moderate reaction conditions, in which the activity and selectivity can be easily adjusted by varying the electrode potentials. In addition, photocatalysis is capable of transferring photonic energy to energetic carriers to drive redox reactions and produce high chemical potential products. This will thus break the thermodynamic equilibrium and make the uphill reactions, such as non-oxidative coupling of methane (NOCM; $2CH_4 \rightarrow C_2H_6 + H_2$) and overall water splitting, occur at room temperature. Besides minimizing energy consumption, these low-temperature methane conversion processes also refrain from coking and sintering of catalysts, as is often suffered in conventional high-temperature thermocatalysis systems. Moreover, the low-temperature processes can produce useful products that a high-temperature system is unable to do. For example, methanol can often be generated in low-temperature POM but is hard to be obtained in high-temperature counterpart because of the tendency of catalytic decomposition. It is thus possible to realize beneficial selectivity in a low-temperature direct route. More encouraging results could be obtained if the superiorities of thermo-, electro-, and photocatalysis can be combined for methane conversion by designing multifunctional catalytic systems that can simultaneously couple the driving forces from thermal, electric, and photonic energies.

Although the rate-determining step of various methane conversion reactions is consistently related to the dissociation of the first C–H bond, the reaction mechanisms of these processes are quite diversified in that they vary with the reaction temperature and systems. High-temperature reactions of commercial importance, like steam or dry reforming of methane, rely on the dissociative adsorption of CH_4 into methyl radical and H on the surface of metal catalysts, which can be interpreted in terms of the Brønsted-Evans-Polanyi relationship.[6] Basically, the mechanisms of C–H bond cleavage of CH_4 at low temperature can be classified into two categories regardless of heterogeneous or homogeneous systems (Figure 2). The first mechanism includes the abstraction of hydrogen from methane to form $\cdot CH_3$ radical by electrophilic oxygen atoms, such as M–O sites on solid catalysts,[7] radicals (•OH, •O–R, etc.),[8] and oxo metal complexes of high-valent metals. In the common electro-/photoactivated reaction processes, electric or photonic energy often promotes the formation of reactive-oxygen-containing species over electro-/photocatalysts to activate the C–H bond of methane through electrophilic processes. The second mechanism involves the formation of metal–CH_3 (M–C) σ-bond as a reaction intermediate. In heterogeneous systems, the M–C σ-bond is formed via the interaction of CH_4 with coordinatively unsaturated metal atoms on solid catalyst.[9,10] In the homogeneous systems, M–C σ-bond is often formed during the activation of CH_4 by molecular catalysts. The coordination of methyl to metal can occur through σ-bond metathesis, oxidative addition, and electrophilic substitution. Unlike the aforementioned radical-like activation process, in this mechanism the metal complex directly cleaves the C–H bond of methane with concomitant coordination with the methyl group.[11,12]

This article will provide a comprehensive overview about the recent progress in direct methane conversion via oxygenation, partial H removal for C–C coupling, or selective functionalization driven by thermal, electric, or photonic energy under mild conditions. The representative catalysts with their operation conditions and C–H activation mechanisms are summarized in Table 1. Interestingly and notably, when looking back at the large-scale methane activation materials irrespectively of reaction systems, those promising catalysts are consistently featured by single active sites consisting of a very limited number of atoms. These single-site catalysts include mono-, bi-, or poly-nuclear transition-metal (TM) sites such as single-atom catalysts (SACs) confined in 2D or 3D materials, TM-exchanged zeolites, metal-organic frameworks (MOFs), and highly dispersed oxide clusters. Moreover, molecular and ionic catalysts are also efficient in homogeneous systems. After highlighting the experimental and theoretical studies of these promising catalysts in direct low-temperature methane conversion, in the end, we conclude with the technological challenges of this active research field and present our perspective on the direction of breakthrough. Low-temperature methane activation can also be assisted by plasma technology. A relevant review has introduced this topic,[13] which will be not dealt with here.

THERMOCATALYTIC METHANE CONVERSION

For direct CH_4 conversion in homogeneous systems, the activation of CH_4 over molecular catalysts is mainly through electrophilic substitution, where the metal ion of the complex attacks methane in polar media to activate the C–H bond and form intermediate M–C bonding. In the heterogeneous systems, unlike the manner that proceeded over metal catalysts in high temperature, direct dissociation of C–H at low temperature is thermodynamically unfavorable; in most cases, the key issue of low-temperature POM lies in the activation of oxidants instead of CH_4 to derive oxidative species that can nucleophilically attack the H of CH_4 to form a methyl radical, which experiences oxygenation or couples together to form a C2 compound. An excellent review recently evaluated the performances of homogeneous and heterogeneous systems (oxides and Fe- and Cu-based zeolites) for direct methane to methanol and emphasized the importance of methanol stabilization in the catalysis.[37] In this section, we briefly overview these traditional reaction systems and then in particular introduce the latest achievements of direct methane conversion over single-site catalysts (SACs or clusters) and MOF-based catalysts.

Direct Methane Oxidation in Homogeneous Systems

A large number of molecular catalysts that biologically modeled the active center were developed to activate C–H bonds at low temperatures. By changing the

Table 1. The Representative Types of Low-Temperature Methane Conversion Systems: Operation Conditions and C–H Activation Mechanisms

Systems	Type of Catalysts	Reaction Conditions						Mechanisms of C–H Activation
		Catalysts	T (°C)	P_{CH4} (bar)	Phases	Oxidants	Products	
Thermocatalysis	noble metals	Au-Pd colloids	≤50	30	liquid	O_2 and H_2O_2	CH_3OOH, CH_3OH, HCOOH, CO_2	radical reaction[14]
	oxides	CeO_x/Cu_2O	177	1.3×10^{-3}	gas	O_2	CH_3OH, CO, CO_2	radical reaction[15,16]
	single-site catalysts	graphene-confined FeN_4	25	18	liquid	H_2O_2	CH_3OH, CH_3OOH, HCOOH, $HOCH_2OOH$, CO_2	radical reaction[17]
		oxide-confined Rh_1O_5	70	28.5	liquid	H_2O_2	CH_3OH, CH_3OOH, CO_2	radical reaction[18]
		zeolite-confined Rh_1O_5	150	20	liquid	O_2 and CO	CH_3OH, HCOOH, CH_3COOH, CO_2	M–C σ-bond[19,20]
		zeolite-confined Pd_1O_4	70	30	liquid	H_2O_2	CH_3OH, HCOOH, CH_3OOH, CO_2	radical reaction[21]
		Cu and Fe-exchanged zeolite	50	30.5	liquid	H_2O_2	CH_3OH, HCOOH, CH_3OOH, CO_2	radical reaction[22]
		MOF-stabilized Fe active sites	50	30.5	liquid	H_2O_2	CH_3OH, CH_3OOH, HCOOH, CO_2	radical reaction[23]
		MOF-stabilized Cu active sites	150	1	gas	O_2	CH_3OH, CH_3OCH_3, CO_2	radical reaction[24]
	molecular catalysts	(bpym)-$Pt^{II}Cl_2$	200	34.5	liquid	H_2SO_4	CH_3OH	M–C σ-bond[25]
Electrocatalysis	noble metals	PdAu/C (fuel cell reactor, cathode)	≥50	0.5	gas	O_2	CH_3OH, CO_2	radical reaction[26]
	oxides	V_2O_5/SnO_2 (fuel cell reactor, anode)	100	0.1	gas	O_2	CH_3OH, CO_2	radical reaction[27]
		NiO/ZrO_2 (fuel cell reactor, anode)	40	1	gas	O_2	CH_3OH, HCHO, CO, HCOOH, CH_3CH_2OH, CH_3COOH, CH_3COCH_3, $CH_3CHOHCH_3$	radical reaction[28]
		$TiO_2/RuO_2/V_2O_5$	RT	0.98	liquid	H_2O	CH_3OH, HCHO, HCOOH	radical reaction[29]
		TiO_2	20	1	liquid	H_2O	CO, CO_2	M–C σ-bond[30]
	ionic catalysts	$PdSO_4$	140	≥6.89	liquid	H_2SO_4	CH_3OH	M–C σ-bond[31]
Photocatalysis	semiconductors	TiO_2/SiO_2	37	0.17	gas	none	C_2H_6, H_2	radical reaction[32]
		$BiVO_4$	55	0.2	liquid	NO_2^-	CH_3OH	radical reaction[33]
		FeO_x/TiO_2	25	2×10^{-4}	liquid	H_2O_2	CH_3OH, CH_3CH_2OH	radical reaction[34]
	zeolites	beta-zeolite	RT	0.64	gas	O_2	CH_3OH, HCHO, HCOOH, H_2, C2	radical reaction[35]
		Zn^+-ZSM-5	RT	1	gas	–	C_2H_6, H_2	M–C σ-bond[36]
	ionic catalysts	$Ce^{III/IV}$ and alcohol	RT	50	liquid	organics	methylated products	radical reaction[8]

RT, room temperature.

relative energies of the molecular orbitals or the polarity, methane can bind with the active metal center properly to enhance the reactivity, which can not only reduce the reaction temperature but also improve the selectivity. In the early 1980s, Shilov et al.[38,39] first reported that methane can be oxidized to methanol and chloromethane (CH_3Cl) by K_2PtCl_4 in the presence of K_2PtCl_6 (Equation 5) with the reaction temperature lowered to 120°C. Noting that the Pt(II) was the active site for methane conversion, which was produced by the oxidant K_2PtCl_6 hydrolysis during the

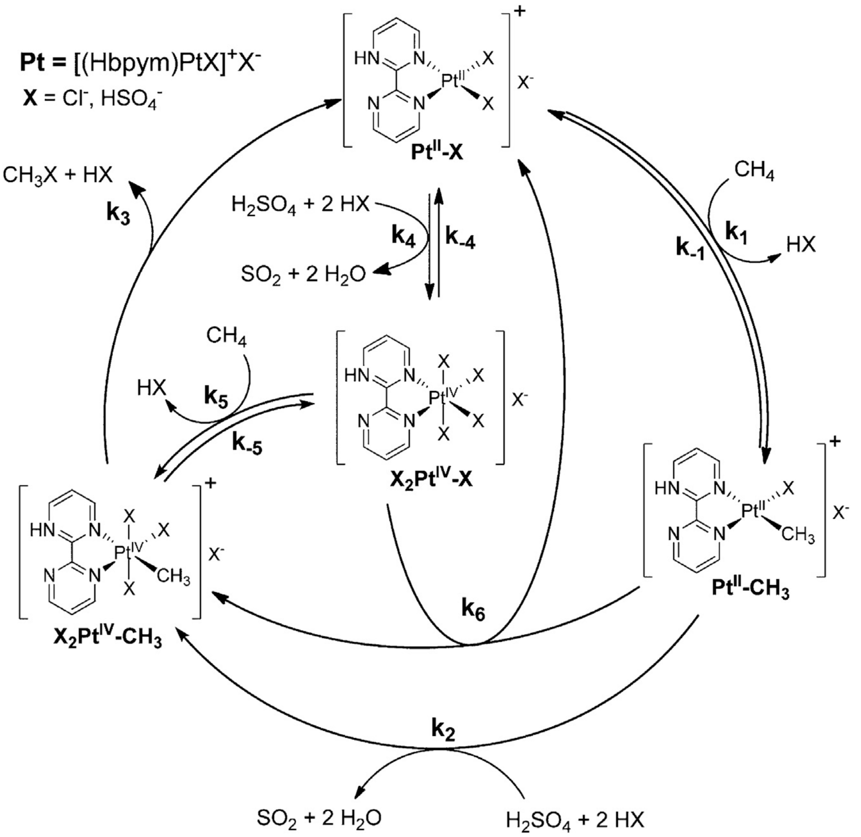

Figure 3. Reaction Process of Methane Conversion with Concentrated H_2SO_4 by the Periana System with [(2,2′-bipyrimidine)$PtCl_2$] as the Catalyst

Reprinted with permission from Mironov et al.[25] Copyright 2013 American Chemical Society.

reaction. Given the low turnover frequency and easy deactivation of the catalyst, this seemingly appealing system has been shelved afterward.

$$CH_4 + H_2O + [PtCl_6]^{2-} \xrightarrow[120^\circ C]{[Pt(H_2O)_2Cl_2]} CH_3OH + [PtCl_4]^{2-} + 2HCl \qquad \text{(Equation 5)}$$

Inspired by the Shilov system, Periana et al.[40] adopted an organic ligand to coordinate Pt(II) to stabilize the active site in the form of [(2,2′-bipyrimidine)$PtCl_2$]. The upgraded catalyst can catalyze the methane oxidation to methyl bisulfate (CH_3OSO_3H) in concentrated sulfuric acid with conversions of methane around 90% and selectivity approximately 81% at 220°C. The concentrated sulfuric acid in this system not only served as the solvent and the oxidizing reagent but also protected the product from over-oxidation by protonation and esterification of methanol to the more stable product CH_3OSO_3H. However, studies showed that the [(2,2′-bipyrimidine)$PtCl_2$] catalyst was sensitive to the by-products of water, and the generated water during the reaction severely suppressed the methane conversion. When the concentration of the H_2SO_4 solvent drops below ~90%, the turnover frequency of the catalyst drops from $10^{-3}s^{-1}$ to $<10^{-5}s^{-1}$. In light of the system's higher stability and efficiency than those of the Shilov system, the authors proposed that the reaction proceeds according to the following three steps (Figure 3):[25] (1) reversible C–H activation by methane coordination on the Pt center to form the (bpym)Pt(II)-CH_3 intermediate (step k_1), (2) (bpym)Pt(II)-CH_3 oxidation to form the (bpym)Pt(IV)-CH_3 species (step k_2), and (3) reductive functionalization of the (bpym)Pt(IV)-CH_3 species to methyl bisulfate (step k_3). Note that (bpym)Pt(II) can be rapidly oxidized to the inactive (bpym)Pt(IV) species (step k_4) by concentrated H_2SO_4 at 200°C according to the Shilov system. However, for the Periana system, the authors demonstrated that the (bpym)Pt(IV) can be brought back to the active (bpym)Pt(II) species by a so-called "self-repair" reaction with the (bpym)Pt(II)-CH_3 generated from C–H activation of methane by (bpym)Pt(II) (step k_5), which was evidenced by quantum-mechanical studies.[25] Subsequently, much effort has been dedicated to improve the Periana system. With the aid of ionic liquids and Pt(II) compounds, methane can be oxidized to methanol and methyl bisulfate at 220°C with a maximum turnover number (TON) of 3.5.[41] In addition, Schüth et al.[42] reported that methane can be oxidized to CH_3OSO_3H with K_2PtCl_4 as an extremely active catalyst, achieving a turnover frequency of more than 25,000 h^{-1} in 20% oleum with selectivity above 98% at 215°C.

Besides the Pt-based catalysts, Hg-based catalysts were also developed in the methane conversion. In 1950, $HgSO_4$ was patented to be active for methane oxidation to yield a mixture of oxidized products (predominantly CH_3OSO_3H) at temperatures between 100°C and 450°C. The methane conversion can reach 44% at 300°C. In 1993, Periana and co-workers reported that mercuric triflate in triflic acid at 180°C can effectively react with methane to selectively generate methyl triflate.[43] The methane conversion was as high as 50% at 85% selectivity to methyl bisulfate (~43% yield). They also proposed a possible catalytic cycle involving three steps: (1) electrophilic C–H activation by $Hg(OSO_3H)_2$ to form CH_3HgOSO_3H species, (2) CH_3HgOSO_3H decomposition to CH_3OSO_3H and $Hg_2(OSO_3H)_2$, and (3) oxidation of $Hg_2(OSO_3H)_2$ by H_2SO_4 to regenerate $Hg(OSO_3H)_2$, which was evidenced by the theoretical calculations.[44] Subsequently, Bell and coworkers screened a series of Hg(II) catalysts in fuming sulfuric acid with oxygen as the oxidant, including Hg_2SO_4, Hg_2Cl_2, $HgSO_4$, $HgCl_2$, $Hg(CH_3COO)_2$, $Hg(CF_3SO_3)_2$, and HgTe.[45] The reaction was conducted at 130°C to prevent oxidation of methanesulfonic acid (MSA). The $Hg(CF_3SO_3)_2$ was found to possess the highest selectivity of 92% for MSA, while HgTe was found to give the highest TON of 104. For the system, the SO_3 concentration exceeding 30 wt % could lead to MSA over-oxidation to CH_3OSO_3H, while a low concentration of SO_3 would decrease the methane conversion.

In addition, Pd-based catalysts were also studied widely during the past years. Firstly, Sen et al.[46,47] found that $PdSO_4$ was also competent for methane conversion to methyl bisulfate in oleum. The TON can reach 15 with H_2SO_4 containing 30% SO_3 at 160°C for 24 h. Then, Michalkiewicz et al.[48] reported that metallic palladium can increase the TON up to 47 at 160°C for 2 h. Further, Periana et al.[49] demonstrated that $PdSO_4$ was active for the direct oxidative coupling of methane to acetic acid in 96% sulfuric acid, in which Pd(II) could catalyze methane oxidation to acetic acid with a 90% selectivity and a TON up to 18 at 180°C. Afterward, Bell and co-workers[50,51] extended on this system by introduction of $CuCl_2$ to enable the use of oxygen as the final oxidant. The selectivity of acetic acid was 57% at 180°C with methane and oxygen as the reaction gas. In addition, Bao and co-workers reported that the use of redox couples for regeneration of palladium acetate catalysts can achieve the selective oxidation of methane to methyl trifluoroacetate in trifluoroacetic acid at 80°C with a TON around 0.7 per hour.[52]

Besides the C1 products, methane can also be converted to C2 products in the aid of CO reaction gas at low temperatures. As early as 1994, Sen and co-workers[53] found that methane can be converted to CH_3COOH in the presence of CO and O_2, with $RhCl_3$ as the catalyst in an aqueous medium at a temperature around 100°C. In this process, CH_3OH and HCOOH were the only by-products observed in solution. The soluble rhodium species, rather than metallic rhodium, is the active site for CH_3COOH formation, which can activate methane to form the Rh-CH_3 intermediates. CO insertion follows to form Rh-$COCH_3$, which can react with water to produce CH_3COOH. In addition, they found that Cl^- and I^- can promote CH_3COOH formation. Afterward, they found that the solvent had a great effect on the reaction rate and product specificity.[54] As the concentration of perfluorobutyric acid increased in water solvent, the reaction rate was found to increase steadily, and the product changed from virtually all acetic acid to methanol derivatives. However, water was essential for the reaction since product could not be formed in pure perfluorobutyric acid. Further study demonstrated that both acetic acid and trifluoroacetic acid accelerated the reaction in the $RhCl_3$ system.[55,56]

More homogeneous systems for methane conversion have been introduced in the other reviews.[38,57] It has been proved that in the homogeneous systems, production protection through the formation of methyl esters in the concentrated acid reaction medium (sulfuric or trifluoroacetic acid) is the key to realizing greatly improved methane conversion and product selectivity. Besides using these corrosive substances, the high cost of these molecular catalysts also limits the practical application of these homogenous systems.

Direct Methane Oxidation in Heterogeneous Systems

Heterogeneous catalysts are more suitable for industrial applications than homogeneous catalysts in view of the convenience for product and catalyst recovery. In this section, after a brief overview of conventional oxide catalysts as well as Fe- and Cu-based zeolite catalysts, the other newly emerged single-site catalysts, including zeolite- and oxide-confined noble-metal SACs, 2D-material-confined SACs and MOFs will be in particular introduced. These single-site catalysts with novel active structures can activate the C–H bond under low temperature or even room temperature. The development of these efficient catalysts characterized by high methane dissociation rates are inspired by the active structure in methane monooxygenase enzymes or the prediction of computational studies.

Oxides and Fe- or Cu-based Zeolites

In very early studies, Mo- and V-based oxide catalysts were firstly developed for heterogeneous methane oxidation, and generally an operation temperature higher than 450°C was needed to obtain appreciable activity in the presence of N_2O.[58,59] Recent progress by Rodriguez and coworkers[15] found that an inverse $CeO_2/Cu_2O/Cu(111)$ catalyst activated methane to produce C, CH_x fragments, and CO_x species at room temperature. The addition of water can convert methane into the only adsorbed CH_x species methanol production with high selectivity. This is because the OH groups from water dissociation adsorbed easily on the active sites and thus inhibited the CH_x full decomposition. Benefitting from the sit blocking effect of water, they further reported a Ni/CeO_2 catalyst to improve the methanol selectivity of methane conversion.[16] With the aid of concentrated acid reaction medium for product protection as used in the homogeneous Periana system, SiO_2-supported gold nanoparticles[60] were reported to be highly efficient for methane oxidation with the aid of [Bmim]Cl ionic liquid, in which the methane was converted to methyl trifluoroacetate with trifluoroacetic acid and trifluoroacetic anhydride as the acidic reagents and $K_2S_2O_8$ as the oxidant. A methane conversion of 24.9% was claimed with a 71.5% selectivity of methanol derivate at 90°C.

Inspired by the active structure in methane monooxygenase enzymes to catalyze methane to methanol, zeolite-stabilized TM (mainly Fe and Cu) centers have been artificially fabricated and show promising methanol selectivity at low temperature.[37,61,62] The exchanged zeolites, such as MOR and ZSM-5, have been studied extensively for methane conversion with proper oxidants (e.g., O_2 and N_2O) in the stepwise or non-stepwise reaction process.

In the stepwise process, the metal-exchanged zeolites are first activated by oxidants at relatively high temperature (450°C –500°C) followed by passing methane at around 150°C–200°C, and then the reaction products are extracted from active sites. The di-copper μ-oxo species[63] and trinuclear copper species are active sites for methanol synthesis, and trinuclear copper species could be formed in the non-framework of the zeolite structure.[64] The di-copper μ-mono oxo active sites were evidenced from the absorption band at 22,700 cm^{-1} in UV-visible (UV-vis) spectra.[63] Since μ-oxo-dicopper active sites form only at higher temperature, most of the studies were done in the stepwise conversion process. In the stepwise processes, the activation step plays a key role in the formation of active sites, and it influences the final methanol yield. Pappas et al.[65] studied in detail the various activation conditions and found that the oxygen treatment done at a higher temperature and longer activation time yielded maximum methanol productivity due to the increased formation of the Cu^{II} active site. Under the optimized reaction conditions, the methanol yield of 125 μmol g^{-1} was achieved for the Cu-SSZ-13 sample. Further, Tomkins et al.[66] avoided the high-temperature activation treatment by applying elevated pressure in the activation step over the copper-exchanged zeolite, which gave the stable methanol yield of 56.2 μmol g^{-1} using 37 bar of methane at 200°C under the isothermal condition. The isothermal condition avoids the time-consuming heating and cooling step during the stepwise cycles. Interestingly, the conventional mono-copper-oxo species is absent, and the smaller copper cluster, which possesses a size of less than 1 nm, was identified as the active site. Sushkevich et al.[67] claimed that water, a cheap oxidant, can be used for the reactivation or regeneration of the catalysts after the first reaction cycle. Water with an inert gas such as helium was used for the reactivation of copper-containing zeolite, and they achieved 0.204 mol of CH_3OH per mole of copper with a high selectivity of 97%. A methane oxidation mechanism was also proposed, i.e., Cu^{II} oxide in the zeolite activates the C–H bond of methane to methanol followed by reoxidation of the Cu^{I} center by water with hydrogen formation. Kim et al.[68] revealed the formation of different types of active centers over a Cu-MOR zeolite sample by activation with N_2O and O_2. The sample activated with N_2O gave a higher methanol production of 97 μmolg^{-1} than the O_2-activated sample (69 μmol g^{-1}) due to the formation of trimeric-oxo clusters in the former case and diverse kind of copper species in the latter case. Interestingly, the sample activated with N_2O showed a linear trend in methanol production with activation temperature, whereas O_2-activated Cu-MOR exhibited a volcano-type plot over a range of temperatures. Grundner et al.[64] developed the well-distributed single-site copper clusters stabilized in the MOR micropore containing $[Cu_3(\mu\text{-}O)_3]^{2+}$ active species, which gave an excellent methanol yield of 160 μmol g^{-1}. This can be achieved by choosing the MOR zeolite with a high aluminum concentration in the side pockets and optimized ion-exchange synthesis conditions.

The next step in the stepwise conversion process is the adsorption of methane over the active sites and the formation of methoxy species, evidenced through the disappearance of the absorption band at 22,700 cm^{-1} related to the di-copper μ-oxo species in the UV-vis spectra. The final step is the extraction of methanol from the catalyst surface, which is considered one of the most important and challenging steps. This step affects the amount of total methanol yield and is generally done by passing steam or some proton resource solvent such as ethanol. For instance, the acetonitrile and water mixture with equal volume was used to extract methanol from the catalysts in the methane oxidation.[69] Starokon et al.[70] demonstrated the importance of water containing solvent medium in the extraction process to get the maximum yield of methanol. Wulfers et al.[71] used the water stream with nitrogen at 200°C as the extraction condition and yielded methanol of 16 μmol g^{-1} for copper-exchanged ZSM-5 samples. Narsimhan et al.[72] modified the conventional extraction method by water, oxygen, and balance methane for the extraction of methanol, and they achieved a methanol yield of 37 μmol g^{-1} for Cu-Na-ZSM-5.

Recently, the direct or non-step methane conversion process at low temperature sparked interest because of the lower space-time yield of methanol in the stepwise conversion processes.[73] For the first time, Narsimhan et al.[72] reported the direct catalytic methane oxidation with oxygen or water at a reaction temperature of 210°C. The effect of water stream on the direct methane oxidation over Fe-ZSM-5 was investigated using N_2O as oxidant.[74] Interestingly, the introduction of stream enhanced the desired product selectivity of methanol from 1% to 16% and inhibited coke formation. The presence of water in the reaction environment favors methanol desorption and inhibits coke formation via the competitive adsorption of water. van Bokhoven and coworkers[75] compared the reactivity of Cu-MOR toward methane conversion with oxygen (aerobic oxidation) or water (anaerobic oxidation) and demonstrated that the oligomeric copper species exhibit high activity under both aerobic and anaerobic conditions, while monomeric copper sites produce methanol in only aerobic processes.

Oxidants other than N_2O and O_2, such as H_2O_2, H_2O, and co-reactants CO and CO_2, were also studied. Hutchings and coworkers[22] studied the selective oxidation of methane to methanol in aqueous conditions by using hydrogen peroxide. The C–H bond of methane was activated over the active site produced from the reaction between Fe-ZSM-5 and H_2O_2 and resulted in the formation of the primary product, methyl hydroperoxide CH_3OOH. This finding was also confirmed by the study over Fe-ZSM-5 catalysts with a different Si/Al ratio.[76] The Cu-exchanged MOR and ZSM-5 were used for the synthesis of acetic acid through a tandem oxidation-carbonylation reaction with methane, and the activity of Cu-MOR was found to be higher than that of Cu-ZSM-5.[77] This is due to the formation of new Cu^{2+} species in Cu-MOR, which oxidize methane and promote the migration of intermediate species to the Brønsted acidic sites of the 8-membered ring for the carbonylation reaction. The Brønsted acid site of zeolite is important for the carbonylation reaction and the acetic acid yield. Wu et al.[78] studied the simultaneous activation of methane and CO_2 into acetic acid over a zinc-modified H-ZSM-5 catalyst through solid-state NMR spectroscopy at the temperature range of 250°C–500°C. They proposed that the zinc sites activate methane to form zinc methyl species (-Zn-CH_3) followed by CO_2 insertion to produce acetic acid via proton abstraction from Brønsted acid sites of the zeolite to -Zn-$OOCCH_3$. Rabie et al.[79] investigated the continuous synthesis of acetic acid in the flow micro-reactor system over the Cu-exchanged M^+-ZSM-5 catalysts where $M^+ = Li^+$, Na^+, K^+, and Ca^{2+} at the temperature range of 425°C–525°C. Among these catalytic systems, Cu-K-ZSM-5 exhibited the highest activity of 395 μmol g^{-1} h^{-1} of acetic acid because of the highest adsorption capacity of CO_2.

Zeolite- and Oxide-Supported Noble-Metal SACs

Although some Fe- and Cu-based zeolites are reported to be able to give almost 100% methanol selectivity, the limited activation ability of these catalysts to C–H bond requires the use of H_2O_2 for the production of methanol with low yield. As extensively confirmed that Rh is among the best catalysts for methane reforming at high temperature,[6] Rh-based zeolites have also demonstrated powerful activity for methane activation under mild conditions with oxygen as the oxidant. Flytzani-Stephanopoulos and coworkers[19] and Tao and coworkers[20] reported the atomically dispersed Rh/ZSM-5 catalyst for direct coupling of CH_4, CO, and O_2 to produce acetic acid in water at temperatures $\leq$ 150°C under elevated pressure. The activity of the Rh atom is >1,000 times higher than that of free Rh cations, and the product selectivity of acetic acid over this catalyst reached ~70%. The active site Rh_1O_5, singly dispersed on the internal surface of the micropores of ZSM-5, is supposed to activate the first C–H bond of CH_4 to form Rh–CH_3 coordination. The Rh–CH_3 bond could be further functionalized through either O insertion or CO insertion to form Rh-OCH_3 or Rh-$COCH_3$ intermediates, respectively.[20] The final hydrolysis of two intermediates gave CH_3OH or CH_3COOH. An isotope experiment also confirmed that the C atom of methyl and carboxyl groups in CH_3COOH are respectively derived from CH_4 and CO.[19] Since the production of CH_3COOH required the successive adsorption and activation of the CH_4, CO, and O_2 at a single Rh atom, over-high pressure of CO or O_2 will saturate the coordination of the Rh atom and thus deactivate this catalyst. HCOOH, the origin of which was not fully explained in both studies, can also be identified in the product. However, CH_4-pressure-dependent HCOOH activity and the related isotope experiment implied that HCOOH possibly came from both the methanol oxidation and hydration of CO. Density function theory (DFT) calculation of minimum-energy paths of CH_3COOH formation from CH_4, CO, and O_2 at the singly dispersed Rh_1O_5 site revealed that the formation of transition states related to C–H bond activation and the transformation of carbonylation intermediates were rate-limiting steps (Figure 4). On the surface of ZrO_2, the dispersed Rh single atoms were also in the coordination form of Rh_1O_5.[18] The Rh SACs on ZrO_2 could catalyze partial oxidation of CH_4 with H_2O_2 into methanol in an aqueous phase at 70°C or direct methane conversion with O_2 to ethane at 260°C.

Pd_1O_4 single-sites anchored on the internal surface of micropores of ZSM-5 also demonstrated excellent performance for methane activation.[21] In the presence of H_2O_2, CH_4 was partially oxidized into methanol over Pd_1O_4 at low temperature (50°C–95°C) with formic acid as the major product. DFT calculations showed that methanol is the thermodynamically stable product over Pd_1O_4. The inconsistency between calculation and experimental result revealed that the formation of formic acid is kinetically controlled. However, with the assist of the CuO co-catalyst, the major product can be shifted into methanol with a selectivity of more than 80%. Similarly, the 0.01 wt % Pd/ZSM-5 yielded the total product of 111.91 mmol with 7.39 mmol of methanol, whereas 0.01 wt % Pd supported on Al_2O_3 and SiO_2 yielded only very few millimoles of oxidized product.[21] Hence, the Pd cations anchored on open surfaces are not active for this transformation. In the case of Pd-ZSM-5, single-site Pd_1O_4, which is present in the micropore of ZSM-5, helped in the formation of methanol, whereas the excess Pd, which is present in the external surface of zeolite, did not alter the activity as well as selectivity of the methanol.

On the CeO_2 surface, a very different configuration of TM atoms was demonstrated.[10] The computational results revealed that on CeO_2(111), two Pd^{2+} cations will substitute one large Ce^{4+} ion (Figures 5A and 5B). The thermodynamically stable configuration under typical oxidative conditions is expected to be a Pd^{2+} positioned at a Pd^{2+}-doped CeO_2 surface site (noted as Pd_1/Pd-dop-II). The superior activity

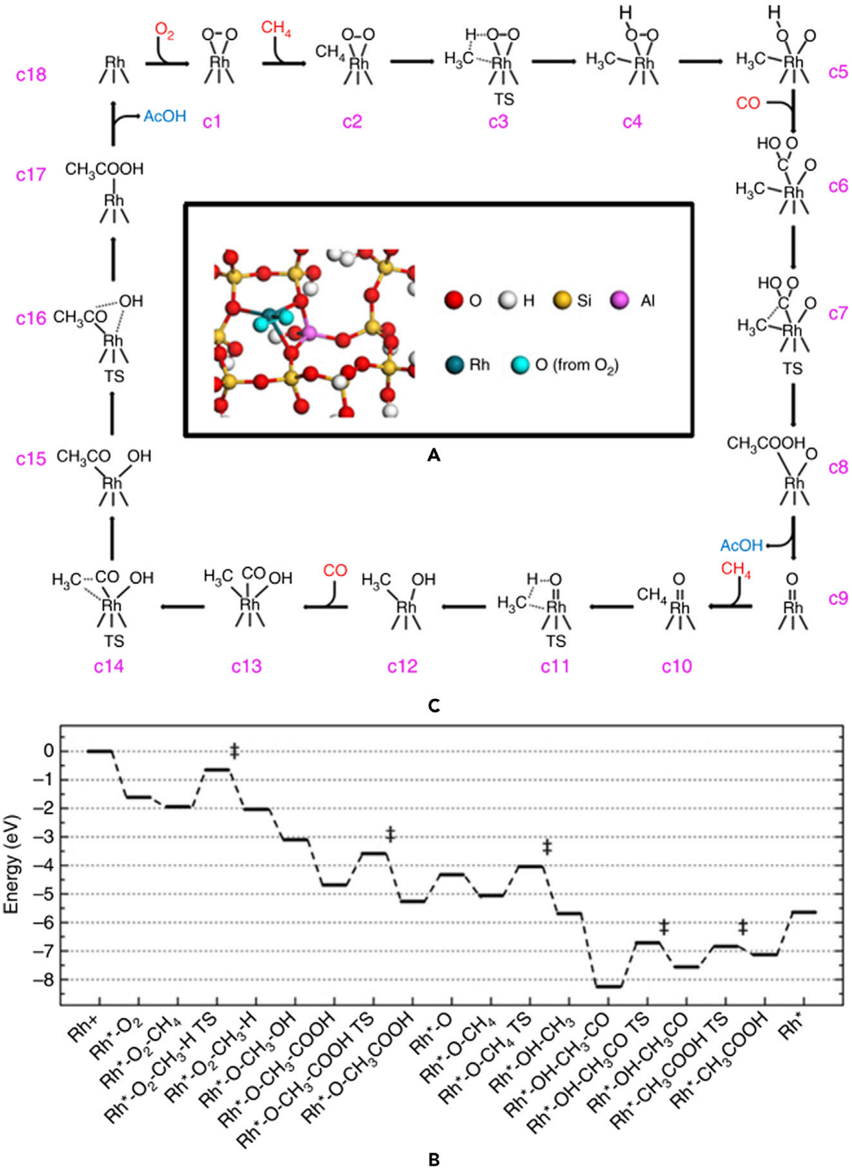

Figure 4. Computational Studies of Reaction Pathways for the Formation of Acetic Acid from CH_4, CO, and O_2 on Rh_1O_5/ZSM-5

The formation of acetic acid is illustrated in a catalytic cycle starting with the singly dispersed Rh_1O_5 site. The balanced reaction cycle consumes one O_2, two CH_4, and two CO to make two CH_3COOH molecules ($2CH_4 + 2CO + O_2 = 2CH_3COOH$).

(A) The optimized catalytic sites, Rh_1O_5 anchored on Brønsted site in microspore of ZSM-5.

(B) Energy profile for the pathway of transforming CH_4, CO, and O_2 to CH_3COOH.

(C) Intermediates and transition states for a complete catalytic cycle, starting with Rh_1O_5 (c1). Transition states are highlighted with the double dagger symbols.

Reprinted with permission from Tang et al.[19] Copyright 2018 Springer Nature.

of this active site originates from a stable 3-fold coordinated exterior Pd by lattice O atoms. The coordinative unsaturation of this Pd atom leads to strong CH_4 chemisorption and activation through the formation of a strong σ-complex similar to the activation process of homogeneous catalysts, as shown in the adsorption and transition states of CH_4 by Pd_1/Pd-dop-II (Figures 5C and 5D) and PdO (Figures 5E and 5F). Electron density analysis showed that there was a redistribution of

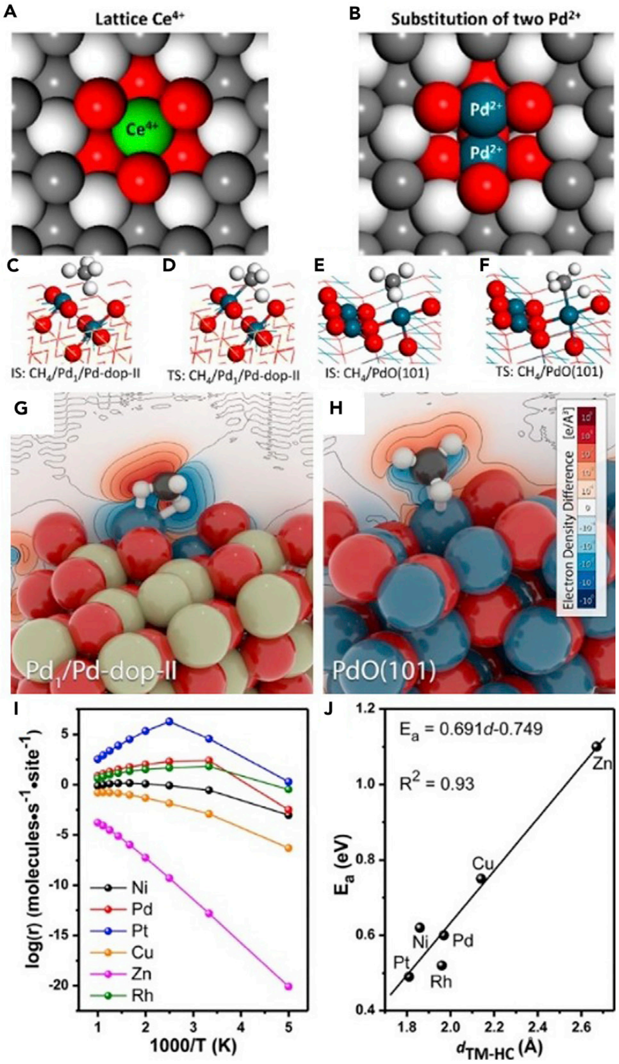

Figure 5. Structure and CH_4 Activation over Pd_1/Pd-dop-II on CeO_2

(A and B) Illustration of the replacement of (A) one lattice Ce^{4+} ion by (B) two Pd^{2+} ions (ionic radii of Ce^{4+} and Pd^{2+} used).

(C and D) Adsorption (C) and transition (D) states of CH_4 by Pd_1/Pd-dop-II.

(E and F) Adsorption (E) and transition (F) states of CH_4 by PdO(101).

(G and H) Electron density difference contours of CH_4 adsorption on Pd_1/Pd-dop-II (G) and PdO(101) (H). Color code: cyan, Pd; red, O; off-white, Ce; gray, C; and white, H.

(I and J) Computed CH_4 dissociation rates for various TM_1/TM-dop-II structures as a function of temperature with P_{CH4} = 0.1 atm (I) and (J) relationship between the CH_4 dissociation barrier and distance between the reactive TM atom and the H atom of the activated C–H bond in CH_4 in the adsorbed state.

Reproduced with permission from Su et al.[10] Copyright 2018 American Chemical Society.

electron density between CH_4 and two types of surfaces (Figures 5G and 5H). The local coordination environment of Pd_1/Pd-dop-II is more favorable for the formation of an O–H bond during C–H bond cleavage. Other TMs such as Pt, Rh, and Ni on CeO_2 give rise to identical structure and high activity for C–H bond activation. The computed CH_4 dissociation rates of these TM_1/TM-dop-II structures decrease in the following order: Pt ≫ Pd > Rh > Ni > Cu > Zn (Figure 5I). The barrier for CH_4 dissociation is closely related to the interaction distance between the TM atom and H atom of CH_4 in adsorbed state (Figure 5J).

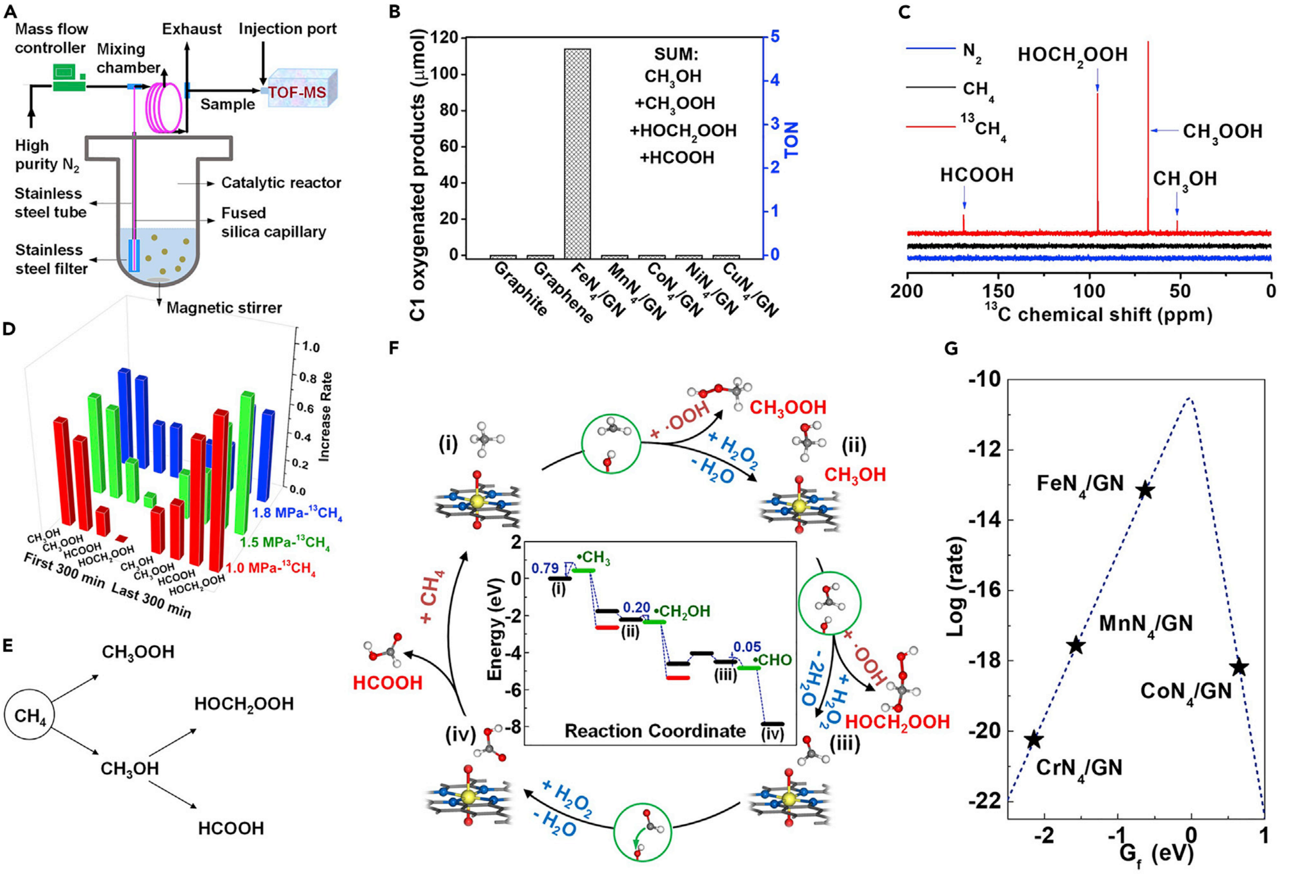

Figure 6. Catalytic Activity and Reaction Mechanism for Methane Oxidation over Graphene-Confined FeN_4 Catalyst

(A) Scheme of *in operando* TOF-MS online connected with high-pressure reactor.

(B) Different catalysts for methane oxidation at 25°C.

(C) ^{13}C NMR spectra obtained from N_2, CH_4, and $^{13}CH_4$ as the reaction gas.

(D) The increase in the rate of the products at 0–600 min detected by *in operando* TOF-MS.

(E) A possible reaction path for methane oxidation over graphene confined FeN_4 catalyst.

(F) Reaction pathway of methane conversion to CH_3OH, CH_3OOH, $HOCH_2OOH$, and HCOOH (the energy of reaction initiation was set as 0 eV) as well as reactants (black), intermediates (blue), products (green and red), and the activation energy of each step (unit, eV).

(G) The relationship between the methane activation rate (log[rate]) and formation energy of the O–MN_4–O active site (G_f) presents a volcano curve. The G_f and activation rate of the calculated O–CrN_4–O, O–MnN_4–O, O–FeN_4–O, and O–CoN_4–O structures are shown on the volcano marked by black stars.

Reproduced from Cui et al.[72] Copyright 2018 Elsevier.

2D-Material-Confined SACs

In recent years, there has been an upsurge in developing novel catalysts based on 2D materials. Previous DFT calculations indicated that methane can be oxidized to methanol with graphene-supported Au_4Pd clusters,[80] single-cobalt-atom catalysts,[81] or two-platinum-atom catalysts,[82] which show graphene-deposited metal nanocluster as a promising heterogeneous catalyst for methane partial oxidation. In addition, Nørskov and coworkers[83] theoretically predicted that calcium-doped molybdenum disulfide was active for methane to methanol. Lately, Deng and coworkers[17] and Bao coworkers[84] reported experimentally that methane can be directly oxidized to C1 oxygenated products at room temperature (25°C). The methane oxidation was carried out in a specifically designed online *in operando* time-of-flight mass spectrometry (TOF-MS) connected to the high-pressure reactor (Figure 6A). Screening from a series of 3d metal–N_4 embedded in the lattice structure of graphene nanosheets, they found that only the FeN_4 catalyst was active for methane to CH_3OH, CH_3OOH, $HOCH_2OOH$, and HCOOH (Figure 6B). As far as we know, this is the first time that $HOCH_2OOH$ was identified as a reaction product in methane oxidation. The selectivity of C1-oxygenated products is around 94%. The control experiments using N_2, CH_4, and $^{13}CH_4$ as the reactant gas indicated that C1-oxygenated products came from the oxidation of $^{13}CH_4$ rather than from the catalyst itself (Figure 6C). The evolution of liquid products traced by *in operando* TOF-MS further demonstrated that methane is first oxidized to CH_3OH and CH_3OOH, and the produced methanol can be further oxidized to $HOCH_2OOH$ and HCOOH (Figures 6D and 6E), which was evidenced by the ^{13}C NMR test showing that $^{13}CH_3OH$ as a reactant can be directly converted into $HOCH_2OOH$ and HCOOH over the catalyst. Combined with DFT calculations (Figure 6F) and electron paramagnetic resonance experiments, the unique O–FeN_4–O structure is proved to be able to active the C–H bond of methane to form a methyl radical. The methyl radical can combine with hydroxyl and hydroperoxide groups to form CH_3OH and CH_3OOH. The CH_3OH can be further converted via the hydroxymethyl radical in line with the NMR and TOF-MS experimental data. Comparison studies between the formation energies G_f of O–MN_4–O active sites demonstrated that among all O–MN_4–O (M = Cr, Mn, Fe, and Co) structures, O–FeN_4–O has a moderate G_f and the highest methane activation rate (Figure 6G), confirming the best activity of FeN_4 in the experimental studies.

Besides direct POM, the FeN_4 active site also demonstrates excellent performance for the catalytic oxidation of other hydrocarbons at room temperature because of the coordinatively unsaturated iron sites confined at 2D graphene.[85] It is interesting that the graphene confined FeN_4 active site has a similar local structure and reaction mechanism to that of cytochrome P450 with an O–FeN_4–SH site in hydrocarbon oxygenation.[11] This is important for graphene confined FeN_4 to realize the methane conversion at room temperature. The diluted intermediate products derived from stepwise methane oxidation are very complicated, which causes great difficulties in the identification of products in liquid phase. This work provided a prototype for the product analysis in direct methane conversion. The *in operando* TOF-MS online connected with the high-pressure reactor can successfully accomplish the qualitative and quantitative identification of products during a reaction. A real-time analysis is important for us to know how methane is exactly oxidized stepwise. This information is important for us to seek new strategies to control the oxidation process as well as the selectivity in methane conversion. Isotopic tracing experiment using $^{13}CH_4$ is also important to confirm the carbon source of oxygenated products since the products in liquid phase with low concentration could be easily contaminated in the experiment.

MOF-Stabilized Fe and Cu Active Sites

Taking advantages of the Periana homogeneous catalytic system with high activity and selectivity, a covalent triazine-based framework coordinated with a platinum solid catalyst was reported by Schüth and coworkers[86] for methane oxidation by SO_3 in concentrated sulfuric acid, which can convert methane to methyl bisulfate with selectivity above 75% at 215°C. This catalyst showed very stable activity with TONs around 300 even after five recycling steps. Osadchii et al.[23] designed a site-isolated mixed-metal MOF, MIL-53(Al,Fe), with a desired antiferromagnetically coupled high-spin species in a coordination environment analogous to that of a methane monooxygenase enzyme with a binuclear Fe active site. The oxo-bridged Fe dimer was supposed to be the active site for methane oxidation to methanol with H_2O_2 because of the low reaction barrier and high stability under reaction conditions (Figures 7A and 7B). Similarly, Lercher et al.[24] found that Cu-oxo clusters stabilized in MOF NU-1000 (Figures 7C–7F) are active for methane oxidation to

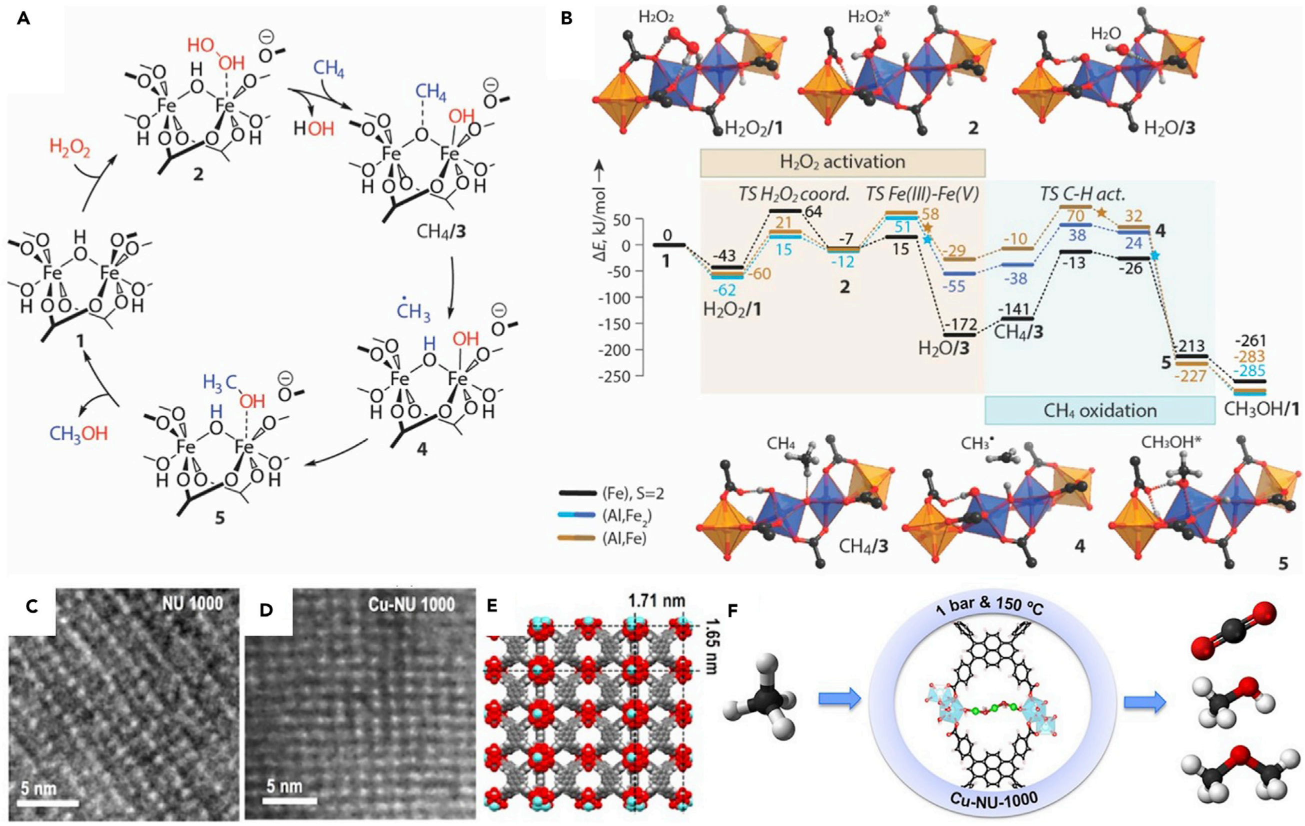

Figure 7. Structure and Catalytic Reaction Mechanism of Fe- and Cu-Based MOFs

(A and B) Proposed mechanism of methane-to-methanol oxidation with H_2O_2 over the dimeric Fe site in MIL-53(Al,Fe) (A) and the DFT-computed minimum-energy reaction path diagrams (including spin transitions indicated with asterisks) for the catalytic process over different Fe-containing MIL-53 models (B). Reproduced with permission from Osadchii et al.[23] Copyright 2018 American Chemical Society.

(C–F) HAADF-STEM images of the polycrystalline NU-1000 (C) and Cu-NU-1000 (D), view of the parent NU-1000 crystal structure looking down the a axis (blue, red, gray, and light-gray spheres represent Zr, O, C, and H atoms, respectively) (E) and scheme of methane oxidation to methanol, dimethyl ether, and carbon dioxide (F). Reproduced with permission from Ikuno et al.[24] Copyright 2017 American Chemical Society.

methanol under mild reaction conditions. The Cu-oxo clusters containing ~15% Cu^+ and ~85% Cu^{2+} undergo partial reduction of Cu^{2+} species into Cu^+ during methane oxidation. The catalyst can convert methane at 150°C with a 60% selectivity to methanol and dimethyl ether with oxygen as the oxidant. These results suggest that MOFs can be a promising class of materials for catalytic methane oxidation. The structural diversity of MOFs allows finely designing reactive metal sites to mimic enzyme systems for efficient methane conversion under mild conditions. Obviously, as has been implied by Cu- and Fe-based zeolite catalysts, MOF-stabilized Cu- and Fe-oxo clusters should be a very interesting type of catalyst in future studies.

In the aspect of theoretical study, hydrogen affinity (E_H) has been shown to be a suitable descriptor to predict the trend of C–H activation ability of several TM oxides. Nørskov and coworkers[7] demonstrated that E_H can be universally used to describe all catalysts that follow the radical-like methane activation, as displayed by the good linear scaling relationship between activation energies and E_H (Figure 8A). Combining this relationship with thermodynamic analysis of active site formation, a complete description of the ability of a catalyst to activate methane considering the influences from both G_H (free energy of H adsorption) and G_f (free energy of active site formation) was established by a 2D rate volcano, showing the rate of methane activation as a function

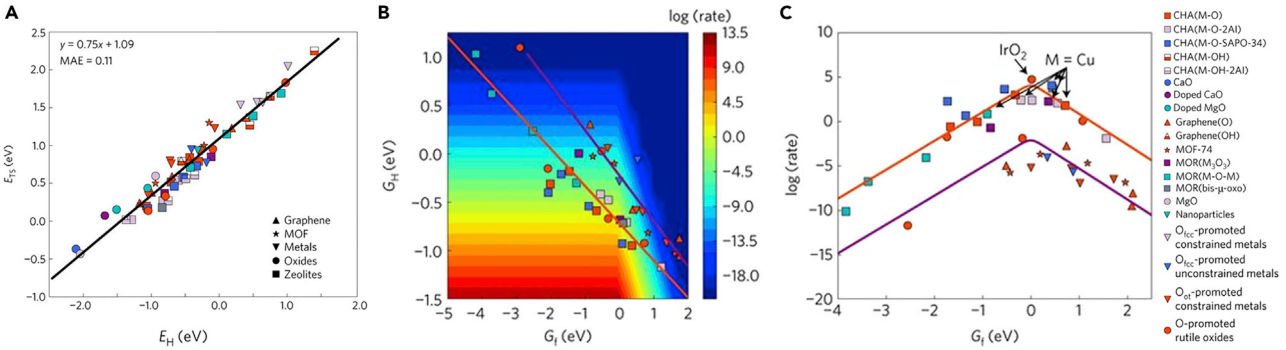

Figure 8. Scaling Relationship for Methane C–H Bond Activation that Proceeds via Radical-like Transition State

(A) Universal scaling relationship between methane C–H bond activation and E_H. Filled symbols correspond to M_mO_x active sites, while half-filled symbols correspond to M–OH active sites. The legend shows the classes of materials explored, and within each class, several metals or cations were considered.

(B) Two-dimensional volcano plot that includes G_H and G_f as descriptors for all explored materials.

(C) One-dimensional volcano plot for the intrinsic rate of methane activation using G_f as a descriptor.

Reproduced with permission from Latimer et al.[7] Copyright 2017 Springer Nature.

of G_H and G_f (Figure 8B). In this 2D volcano plot, all the investigated catalysts separately distribute along two lines. The origin of the two lines seems related to the characteristics of catalyst substrates (red line, zeolite-based catalysts; purple line, oxides and other catalysts). When converting the two lines into a 1D rate volcano showing the relationship between rate of methane activation and G_f, the prediction work becomes much simplified, and it is clear that G_f could be also used as a descriptor to predict the C–H activation barrier of catalysts (Figure 8C). For different types of catalysts, the heights of their corresponding volcanoes could be different, but all these volcanoes will have a peak rate at $G_f = 0$. The G_f is applicative for a very wide range of catalyst classes, including zeolites, oxides, graphene confined TM atoms, MOFs, nanometals, etc. In comparison with hydrogen affinity E_H, G_f is solely associated with the physical structure of the catalyst and thus can provide a more direct prediction to the active site performance of new catalysts. This descriptor perfectly predicted the outstanding performance of IrO_2, which lies close to the peak of the volcano, for low-temperature methane oxidation. The latest surface chemistry study by Weaver and coworkers indicated that methane adsorbed on the IrO_2(110) under ultrahigh-vacuum conditions underwent highly facile C–H bond cleavage at temperatures as low as −123°C.[9] With reaction temperature increasing, the CH_4-derived fragments react with surface oxygen to form carbon dioxide, carbon monoxide, and water, with the carbon dioxide and carbon monoxide products desorbing between 127°C and 327°C. On the basis of recent studies, Nørskov et al. further proposed several strategies to get optimized trade-off between selectivity and conversion in methane conversion to methanol.[87] The strategies include (1) using catalysts with strong methanol adsorption as “collectors” to lower the partial pressure of methanol in gas-phase reaction systems, (2) employing aqueous reaction conditions, or (3) using diffusion-limited catalysts (e.g., highly porous materials). The aim of these strategies is to restrict the migration of products to the active sites for deep oxidation and keep high product selectivity.

ELECTROCATALYTIC METHANE CONVERSION

Low-Temperature Fuel-Cell-type System

Direct methane conversion can be realized by electrocatalysis in a gas-solid reaction system on the basis of fuel cell reactor at low temperature. The reaction system is constituted by cathode and anode separated by ion-exchange electrolytes. The products of electrocatalytic CH_4 oxidation can be tuned by changing the applied bias from the external electric circuit to generate CH_3OH, HCHO, HCOOH, and CO from POM and C_2H_6 or C_2H_4 from OCM. The conversion of methane and product selectivity are determined by reaction temperature, catalysts, applied bias (or current), and gas-feeding manner. The key in designing such reaction systems is that both the solid electrolyte and the catalysts should have high ionic conductivity and CH_4 activation ability, respectively, at low temperature. Recently, Wang and coworkers[88] summarized the electrocatalytic methane conversion in both high- and low-temperature fuel cell systems. As a prototype of excellent low-temperature proton conductor, In^{3+}-doped SnP_2O_7 ($Sn_{0.9}In_{0.1}P_2O_7$) has been used as the electrolyte in a H_2–O_2 fuel cell for methane oxidation at operation temperatures between 50°C and 250°C (anode, Pt/C catalyst and H_2 gas; cathode, Pd-Au/C catalyst and CH_4 + O_2 gas).[26] With increasing reaction temperature, the CH_4 conversion is increased and CH_3OH selectivity is decreased. However, the CO_2 formation is prevailing and shows much higher selectivity than CH_3OH. The highest formation rate of CH_3OH is reached over the optimized catalyst with Pd/Au = 8:1 at 250°C with a 6.03% CH_3OH selectivity. Since the bimetallic Pd-Au has been verified as an excellent catalyst for the production of H_2O_2 in both electrocatalytic and thermocatalytic oxygen reduction,[89–91] thermally activated oxygen is also involved in this electrocatalytic system and contributes to CH_4 conversion. Adding Cu to Pd-Au/C delivered similar CO_2 production but obviously improved CH_3OH formation rate.[92] By screening a variety of non-platinum metal oxide anodes, V_2O_5/SnO_2 has been found to be the best material for selective CH_4 oxidation to CH_3OH.[27] To improve the current efficiency for CH_3OH production, the gas feeding was changed, where CH_4 and water vapor mixture was supplied to the anode chamber and air to the cathode chamber. At 100°C, the selectivity and current efficiency toward CH_3OH reached 88.4% and 61.4%, respectively. It is supposed that a strong interaction between highly dispersed V_2O_5 and SnO_2 support leads to partial reduction of V_2O_5 into V^{4+} species that serve as the active site of water oxidation into anion oxygen radicals for electrochemical methane oxidation.

To further decrease the operation temperature, a CO_3^{2-} anion-exchange membrane was used in a fuel-cell-type reactor for electrochemical methane oxidation at room temperature (anode, NiO-ZrO_2 catalyst and CH_4 gas; cathode, $Ca_2Ru_2O_7$ catalyst and CO_2 + O_2 gas).[28] At the cathode side, reaction of CO_2 and O_2 produced CO_3^{2-}, which then traveled across the anion-exchange membrane to the anode. At the anode side, the NiO–ZrO_2 bifunctional electrocatalyst activated CH_4 at room temperature to produce various oxygenates. The oxygen donor, CO_3^{2-}, was adsorbed by the acidic sites of ZrO_2 and donated to electrocatalytically active sites on NiO where CH_4 was activated. Basically, electrocatalytic methane conversion can be realized in any of the present low-temperature fuel cell systems if the proper catalyst, being able to activate methane at low temperature, can be coupled.

Methane Conversion in Liquid-Phase Electrolyte

This kind of reaction system employed the commonly used electrochemical reactors, where the dissolved CH_4 in the liquid phase is oxidized by solid electrodes at low temperature. The reaction medium and electrodes will thus influence the reactivity of the electrochemical system. Surendranath and coworkers[31] introduced rapid electrochemical functionalization of methane to the methanol precursors through the electro-oxidation of the $Pd^{II}SO_4$ catalyst in concentrated sulfuric acid at high methane pressure. The reaction system is exactly analogous with the thermocatalytic Periana system that uses molecular catalysts (2,2′-bipyrimidyl)platinum(II) dichloride to process the same chemistry in similar reaction medium. In both systems, the sulfuric acid medium acts as the solvent (or electrolyte) and oxidant, which also protects methanol precursors from over-oxidation due to the electron-withdrawing nature of $–OSO_3H$ or $–SO_3H$ substituent. The key to methane conversion in these systems is the sustainable generation of electrophilic high-valent metal species to break the C–H bond through the reoxidation of their reduced form in the catalytic cycle, which is, however, rather sluggish and rate limiting in thermocatalysis systems. The electrocatalytic re-oxidation provided a straightforward method to solve this kinetic challenge. Under anodic polarization, electrochemical oxidation of $PdSO_4$ in concentrated sulfuric acid generates a putative $Pd_2^{III,III}$ species. This high-valent Pd complex could rapidly activate methane with a low barrier. The turnover frequencies of methane functionalization reached 2,300 h^{-1} at 140°C, 20-fold higher than state-of-the-art catalysts under pure thermal conditions. It is also identified that the electrocatalytic reaction (faradic pathway) is accompanied by a more efficient non-electrocatalytic process (non-faradic pathway) catalyzed by $Pd_2^{III,III}$, and the two pathways respectively led to the formation of methyl bisulfate (CH_3OSO_3H) and methanesulfonic acid (CH_3SO_3H) in a ratio of ~1:14. This study encouraged that the rate-limiting redox step in thermocatalysis can be potentially overcome if such reaction processes can be adapted into electrochemical systems to facilitate electron transfer by electrochemical polarization.

Although appreciable performance has been accomplished, the strong acid medium also brings about a serious problem for practical application. Li et al.[30] studied the photoelectrochemical CH_4 oxidation on TiO_2 in NaOH aqueous solution electrolyte under ambient conditions and showed that CO can be selectively produced with carbonate as a by-product. At moderate potential (0.4 V versus reversible hydrogen electrode [RHE]), CO selectivity reached 81.9% in the overall oxidation products of methane. Oxidation of CH_4 on the TiO_2 photoelectrode started with photoexcitation of the electron from O^{2-} to Ti^{4+} to produce $^{-\bullet}O–Ti^{3+}$ under illumination, and subsequently, the oxygen radical $O^{\bullet-}$ abstracted the first H from CH_4 to form $Ti–O–CH_3$ (Figure 9). Two adjacent Ti sites on TiO_2 synergistically controlled the overall CH_4 oxidation process. The selectivity of the final oxidation product was closely related with the surface state of TiO_2, and the desired CO selectivity was favored by the Ti^{3+} species, which promoted the switching of C=O–Ti to O=C–Ti. Without this switching process assisted by Ti^{3+}, CH_4 was preferentially over-oxidized into CO_2. As revealed by electron paramagnetic resonance analysis, TiO_2 fabricated by atomic layer deposition possessed the highest concentration of Ti^{3+} species and showed the best performance, while commercial TiO_2 samples (P25 or anatase form) having a low amount of Ti^{3+} delivered a significantly lower yield of CO. Moreover, unlike conventional electrochemical systems, illumination was indispensable in order to observe CO in products, which was possibly because a great deal of Ti^{3+} species were generated upon the photoexcitation.

A severe problem yet to be solved is the extremely low solubility of methane in aqueous solution, which limits the conversion of methane in the common electrocatalytic studies carried out in neutral and alkaline media. Although non-polar mediums can increase methane solubility in liquid electrolytes, these organic solvents would be more easily electro-oxidized prior to methane. A gas diffusion electrode with a porous structure could significantly increase the numbers of gas-liquid-solid interfaces and is particularly favorable for efficient electrocatalytic methane oxidation. A TiO_2/RuO_2/PTFE gas diffusion electrode has been used for electrocatalytic methane oxidation in neutral aqueous electrolyte.[29] The formation rate of methanol reaches 206 mg L^{-1} h^{-1} cm^{-2} with ca. 27% current efficiency at 2 V versus saturated

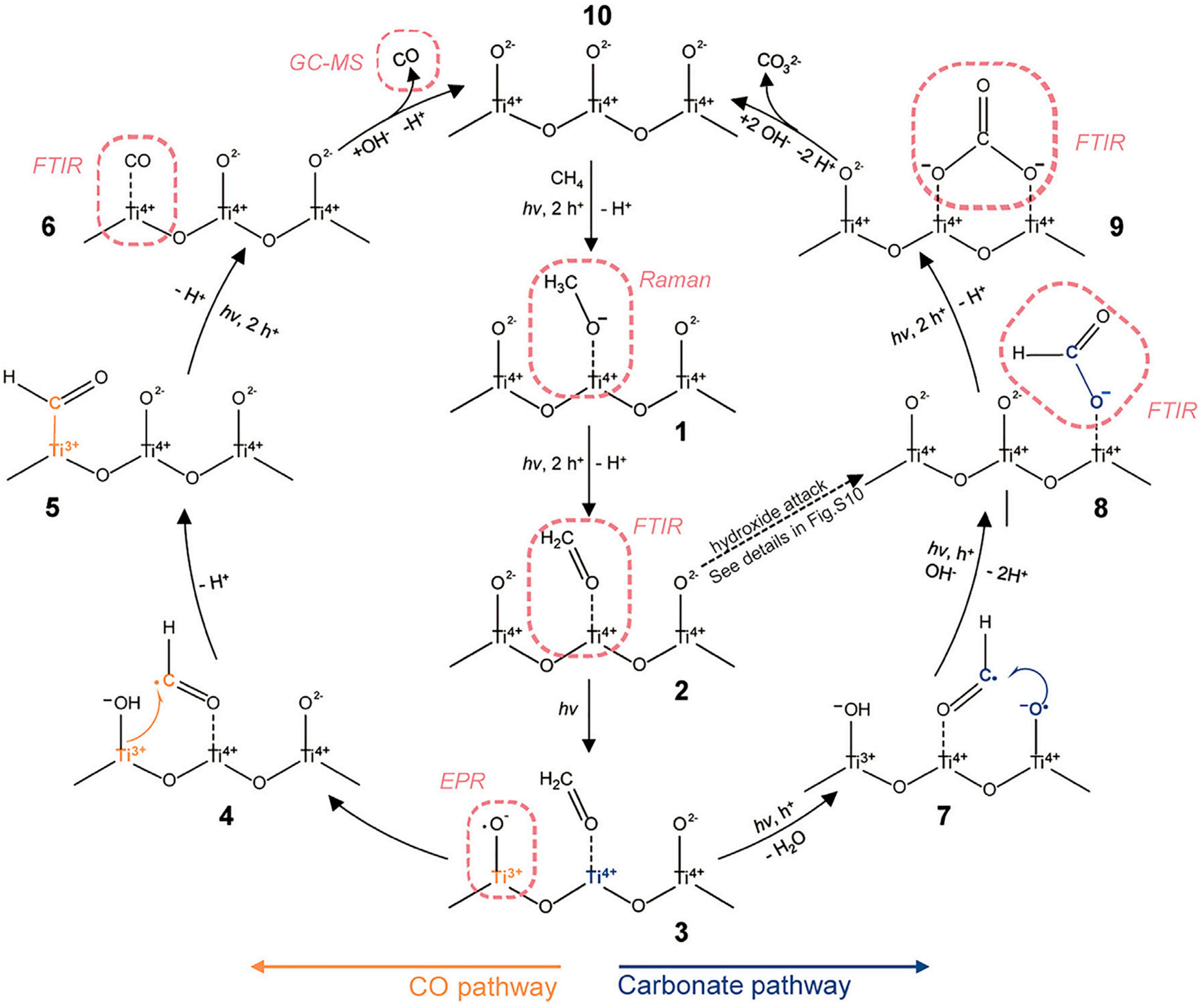

Figure 9. Proposed Mechanisms of Photoelectrochemical Oxidation of CH_4 on TiO_2

The species highlighted by dotted circles have been confirmed by various spectroscopic techniques. The key distinguishing step is identified at the bottom of the catalytic cycle, where the synergistic effect between two adjacent Ti sites promotes the switching of C=O–Ti to O=C–Ti, leading to selective formation of CO. Alternatively, in the absence of such a switching, CO_2 is the preferred oxidation product. Reprinted with permission from Li et al.[30] Copyright 2018 American Chemical Society.

calomel electrode (SCE). Further incorporation of V_2O_5 into the TiO_2/RuO_2/PTFE boosts the formation rate of methanol and current efficiency up to 594 mg L^{-1} h^{-1} cm^{-2} and ca. 57%, respectively, at the same potential with a negligible amount of HCHO and HCOOH formation. According to the existing theoretical and experimental results, SnO_2 and TiO_2 are promising candidates for electrochemical methane oxidation because of the low C–H activation energy[93] and low oxygen evolution selectivity in aqueous solution.

PHOTOCATALYTIC METHANE CONVERSION

Heterogeneous Photocatalytic System

Stable oxide semiconductors, such as Ti-, Ta-, Ga-, and Ce-based oxides, as well as their highly dispersed species on high-surface-area SiO_2 are generally used in heterogeneous photocatalytic methane conversion. These UV-light-responsive semiconductors have wide band gaps with much positive valence band potentials consisting of O2p orbitals (ca. +3 V versus standard hydrogen electrode [SHE]), ensuring a very strong oxidation ability upon photoexcitation. Heterogeneous photocatalytic methane conversion at present are mainly carried out in gas phase systems. The methane is considered to be photoactivated through electrophilic removal of the first H to produce methyl radicals by the hole center $O^{\bullet -}$ ($O^{2-} + h^{+} \rightarrow O^{\bullet -}$) of oxide semiconductors, hydroxyl radicals, or other electrophilic oxygen species. The mechanistic study of photocatalytic POM in the current research is still very inadequate, especially in the determination of active species for C–H activation. The major products in the gas phase reaction systems generally comprise H_2, C_2H_6, CO, and CO_2, while oxygenate products such as methanol are seldom observed in gas phase because they are readily absorbed and reacted with the energetic oxidation species at the photocatalyst surface. Therefore, in gas-phase reaction systems, the over-oxidation of CH_4 often makes the reaction product unselective. In both photocatalytic POM and NOCM systems, the C_2H_6 can be produced from the coupling of methyl radicals. Since the lattice oxygen and surface absorbed oxygen on the photocatalysts are frequently involved in the realistic conditions, substantial CO_2 will be produced unintentionally in photocatalytic methane conversion even in anaerobic photocatalytic reaction space. Involvement of reactive oxygen species will lead to a lower H_2/C_2H_6 ratio, which can be used as an indication of the extent of POM in a NOCM system. A common case is that as photo-oxidation proceeds, notable activity decay can be observed when the reactive oxygen species are gradually depleted. Employing non-reducible wide-band-gap oxide semiconductors could improve such condition because these kinds of materials are free of active oxygen species and not inclined to trap electrons and protons on their surfaces.

NOCM is more advantageous than POM in reaction selectivity control since the addition of oxygen in POM often leads to diversified products, including undesired CO and CO_2. In order to accomplish a genuine and selective photocatalytic NOCM with equimolar ethane and hydrogen evolution, reactive oxygen species must be strictly removed from both the reaction system and the catalyst surface. A Zn^{+}-modified ZSM-5 zeolite photocatalyst was fabricated through a solid-vapor reaction between a dehydrated HZSM-5 zeolite and metallic zinc vapor.[36] Since this material is prepared in a highly reductive condition, involvement of oxygen on the catalyst in the further NOCM reaction can be excluded. Under UV-light irradiation, Zn^{+}-modified ZSM-5 exhibited a stable and much higher methane conversion rate than Ga_2O_3 and mesoporous silica MCM-41, two conventional photocatalysts effective for the NOCM reaction (Figures 10A and 10B). More importantly, the catalytic reaction led to the formation of nearly equimolar ethane and H_2. The selectivity of C_2H_6 was almost 100% and no detectable carbon oxides were produced. Mechanistic studies suggested the overall catalytic cycle was driven by a two-stage photoexcitation process, where light of wavelengths shorter than 390 nm excited electrons from the zeolite framework to Zn^{2+}, and visible light promoted the reactivity of Zn^{+} toward methane (Figure 10C). Computational studies demonstrated that in the optimized structure of the initially adsorbed methane molecule at the Zn^{+} cation in the pore of zeolite, three hydrogen atoms of the methane molecule were attracted by the Zn^{+} cation (Figure 10D). It is proposed that transfer of the visible-light-excited 4s electron of the Zn^{+} to an empty C–H σ*-antibonding orbital of methane mediated the activation of C–H bond, which is a key step in the overall reaction (Figure 10E).

To date, the study on the kinetic mechanism of photocatalytic methane conversion in gas phase is quite insufficient.[94] A simplified description of the reaction mechanism based on the redox process driven by the conduction-band electrons and

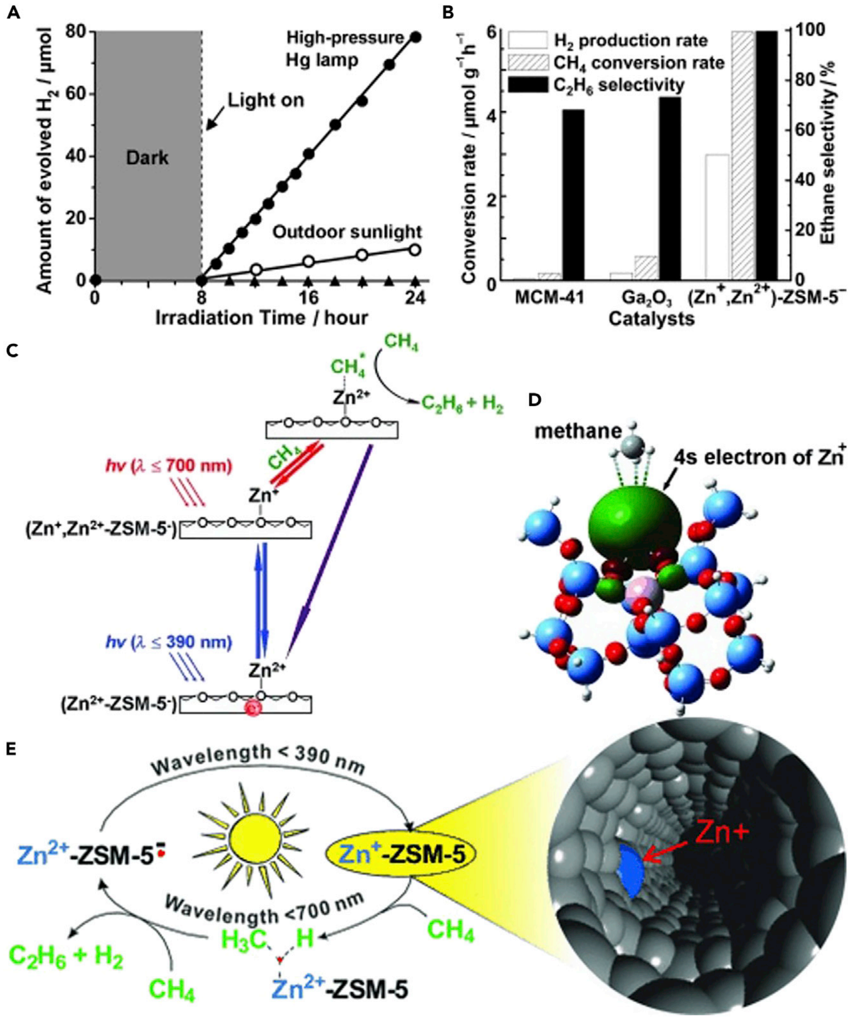

Figure 10. Photocatalytic NOCM Zn^+-Modified ZSM-5 Zeolite Photocatalyst

(A) Photocatalytic hydrogen evolution from the NOCM reaction catalyzed by Zn^+-modified ZSM-5 under high-pressure Hg lamp (full circles) and sunlight irradiation (empty circles). The activity of Zn^{2+}- ZSM-5 under high-pressure Hg lamp is negligible (full triangles).

(B) Methane conversion rate, hydrogen production rate, and ethane selectivity obtained for the NOCM reaction catalyzed by different photocatalysts.

(C) Schematic energy diagram for the processes of the photocatalytic reaction.

(D) The optimized geometry of the adsorbed methane molecule attracted by the Zn^+ active site (red, O; blue, Si; pink, Al; gray, C; white, H; and green, the 4s electron of Zn^+).

(E) Mechanism of photocatalytic NOCM.

Reproduced with permission from Li et al.[36] Copyright 2011 Wiley-VCH Verlag GmbH & Co. KGaA, Weinheim.

valence-band holes is unable to provide detailed understanding of the catalytic process. In addition, the product yields from methane conversion in the gas-phase system are still very low. Photocatalytic POM in liquid phase at elevated pressure is a subject of bigger perspective. For photocatalytic POM in liquid phase at room temperature, besides the common products frequently obtained in the gas phase reaction system, very useful oxygenated products, such as methanol and formic acid, can be delivered. The hydroxyl radical is often a double-edged sword in the reaction. On the one hand, it is proposed to be the active species for methane activation. And on the other hand, excessive hydroxyl radicals would lead to deep oxidation of the methane, when the selectivity of CO_2 and C_2H_6 in gas phase will be increased and selectivity of oxygenated products in liquid phase will be decreased. Therefore, a proper amount of hydroxyl radical in the reaction medium seems important to compromise the methane conversion and methanol selectivity to get the ideal product yield.

Some semiconductors have been studied for the photocatalytic methane oxidation in liquid phase. In a flow-type reactor, $BiVO_4$ is proved to be a promising photocatalyst for POM to methanol under UVC-visible irradiation at 55°C with low CO_2 formation.[95] Introducing electron scavengers such as O_2 and Fe^{3+} into the reaction system will concurrently increase the numbers of holes, thus resulting in the formation of highly oxidative species to increase the oxidation degree of methane and CO_2 formation. In the meantime, a large amount of methyl radicals generated after removing the first H of methane will diffuse into the gas phase and couple together to form C_2H_6. It is interesting that even in pure water or aqueous solution only containing Fe^{3+}, the UVC irradiation can mediate the methane oxidation through hydroxyl radicals derived from direct water photolysis or photo-oxidation of water by Fe^{3+}. However, addition of nitrite ions (NO_2^-) into the $BiVO_4$ suspension gives an opposite trend for photocatalytic methane to methanol.[33] First, nitrite ions serve as UV-filtering agents and are able to weaken water photolysis into hydroxyl radicals. Second, nitrite ions can be a source of scavenger of hydroxyl radicals to control the extent of the oxidation process. In a comparison study using a WO_3 photocatalyst, it was found that both surface fluorination of the photocatalyst or addition of H_2O_2 led to the increase of hydroxyl radicals in reaction systems, which decreased the yield of methanol and increased the yield of C_2H_6 and CO_2. Therefore, any process that will potentially increase the oxidation ability of reaction systems, such as adding electron scavengers, a modulation of the surface property of photocatalysts, and direct use of H_2O_2 as the source of hydroxyl radicals, should be carefully controlled in liquid-phase heterogeneous photocatalytic systems. In the presence of H_2O_2, a recent study using TiO_2-supported iron species as a photocatalyst realized selective oxidation of methane to methanol at room temperature.[34]

Under UVC irradiation, pure beta zeolites display activity for methane photo-oxidation through the homolytic cleavage of hydroxyl groups.[35] The resulting silyloxyl radicals (Si–O•) then abstract H from methane to form methyl radicals. However, CO_2 is much more prevailing than the other products, indicating a high degree of methane oxidation over beta zeolites. Under similar reaction condition to the above-mentioned $BiVO_4$,[95] the formation of over-oxidized products, C_2H_6 and CO_2, can be suppressed with the methanol yield almost unchanged after dispersing Bi and excessive V precursors onto high-surface-area beta zeolites.[96] It has been verified that V_2O_5 incorporation modulated the acid-base surface properties and mitigated Si–OH groups, thus significantly decreasing the selectivity of undesired CO_2. Formation of a $BiVO_4/V_2O_5$ heterojunction on beta zeolites also enhanced photocatalytic activity.

In a flow-type photochemical reaction system, methanol was produced from methane oxidation by hydroxyl radicals derived from the direct photolysis of H_2O_2 by UV light.[97] It was found that only a constant H_2O_2 dosing at low concentrations was sufficient enough to get optimal methanol production. Excessive hydroxyl radicals in the aqueous medium did not improve the methanol production but obviously enhanced HCOOH formation. The study also showed that for a specific dosing rate of H_2O_2, the methanol formation was in equilibrium with methanol oxidation to HCOOH and CO_2, and thus the formation rate of methanol remained constant in a flow-type system. Under continuous light irradiation, the products in a batch-type reactor are likely to be stepwise dehydrogenated through photooxidation by accumulated oxidative species if the reaction duration is long enough. A flow-type reactor possibly prevents such drawbacks and delivers less oxidized products.

Because of the unique catalytic and optical characteristics, nanometals play very important roles in solar-to-chemical energy conversion. Recently, photoenhanced thermocatalytic reactions over nanometal catalysts emerged as a new avenue toward the activation of many useful and tough reactions.[98] Energetic hot carriers (electrons and holes) in photoexcited metallic nanostructures would participate in photochemical activation of reactants, which enables the thermocatalytic reactions to proceed at a lower temperature and, moreover, achieve much higher activities in comparison with pure photocatalytic conditions. Therefore, taking advantages of optical and catalytic properties of nanometal catalysts, more efficient methane conversion, such as steam reforming of methane or dry reforming of methane at relatively lower temperature can be realized.[99,100] Rh nanometal is an outstanding catalyst for reforming of methane.[6] It also displays unique optical properties with strong plasmonic behavior in UV region and interband transition in visible-light range.[101] Visible-light-enhanced steam reforming of methane was observed over a TiO_2 supported Rh nanometal catalyst at a mild operation temperature.[100] Under visible-light irradiation, hot electrons excited in the interband transition of Rh nanoparticles are transferred to the adjacent TiO_2 support, leaving an electron-deficient $Rh^{\delta+}$ state on the nanometal catalyst, which promotes the activation of the C–H bond of methane. The linear relationship between H_2 production and visible-light intensity, and the wavelength-dependent apparent quantum efficiency indicated that the enhanced methane conversion was driven by the hot carriers from the interband transition of Rh nanometals. The larger kinetic isotope effect (rate(CH_4)/rate(CD_4)) over the Rh/TiO_2 hybrid under visible light than under the pure thermal condition (dark condition) validated that the hot carriers played the role in facilitating the rate limiting methane activation. It has also been shown that the apparent activation energy under light irradiation is much lower than that in the pure thermal condition, which further evidenced that excitation of hot carriers assisted methane activation. In addition, enhanced methane activation by excited hot carriers is also involved in other methane reforming systems with diversified single metal and bimetal nanocatalysts.[99,102,103]

Utilizing energetic photons, heterogeneous photocatalysis has demonstrated the ability to drive methane activation at room temperature only with O_2 or H_2O as the oxidant. Such a reaction system shows a greater advantage than H_2O_2-based catalytic systems because H_2O_2 is much more expensive than the oxygenated products. For liquid phase reaction, it is also necessary to enhance the efficiency of methane conversion with elevated pressure to increase its concentration in liquid phase. Efficient photocatalytic methane conversion also requires both strong UV irradiation and sufficient irradiation area. Unlike heterogeneous photocatalysis, thermo- and electrocatalysis do not have such limitations and the methane conversion may occur at the large internal surface of catalysts.

Homogeneous Photocatalytic System

A recent breakthrough employed inexpensive cerium salts as homogeneous photocatalysts and realized efficient and selective functionalization of methane, ethane, and higher alkanes at room temperature under visible-light irradiation.[8] In this homogeneous system (Figure 11), firstly, simple alcohols act as hydrogen atom transfer (HAT) catalysts and transiently coordinate with cerium salts to generate a

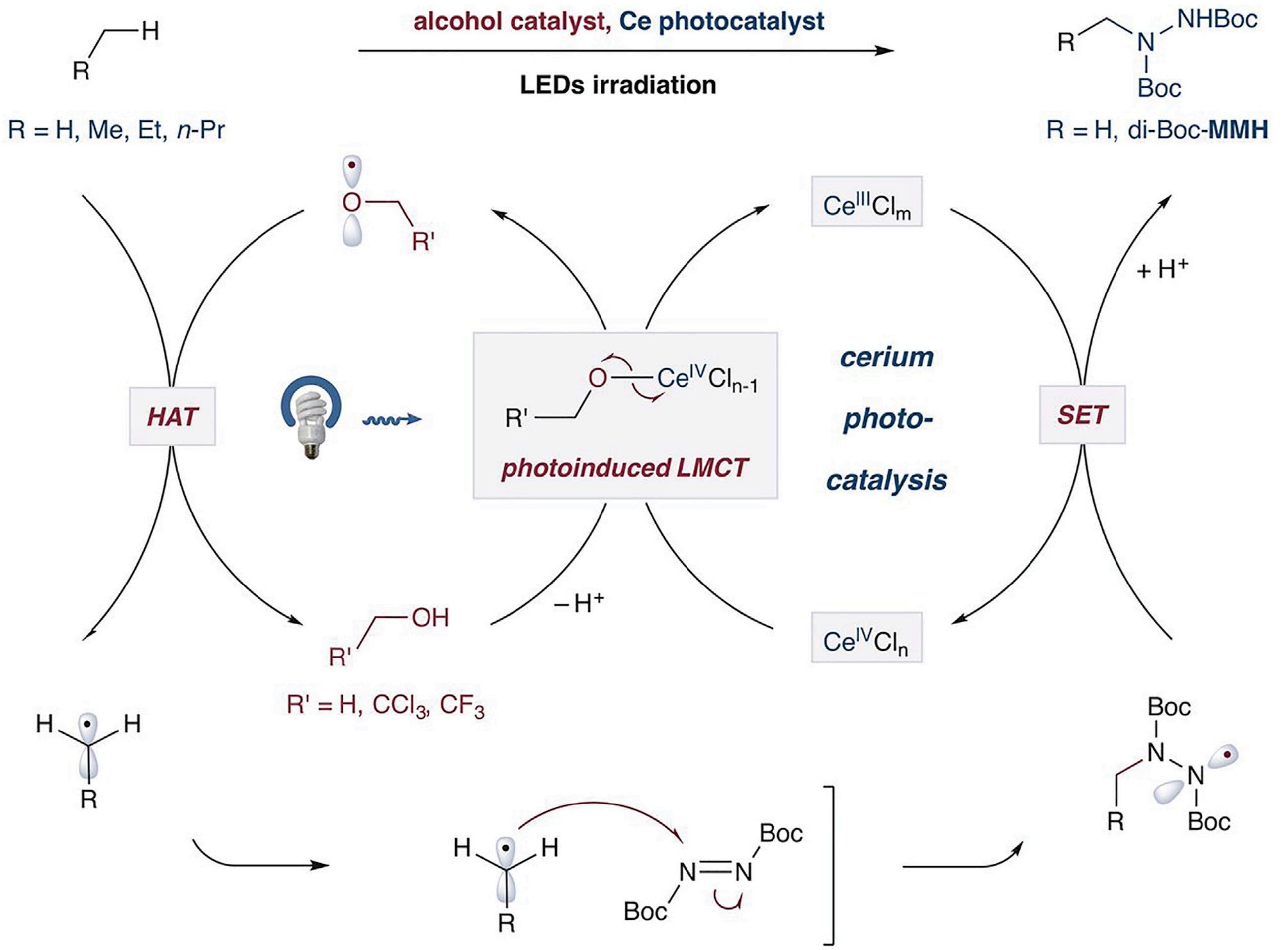

Figure 11. Proposed Mechanism for Cerium-Catalyzed $C(sp^3)$–H Functionalization of Methane and other Gaseous Alkanes

Highly electrophilic alkoxy radicals, generated from simple alcohols via photoinduced LMCT, are employed for the HAT activation of challenging C–H bonds in light alkanes. di-Boc-MMH, di-*tert*-butyloxycarbonyl monomethylhydrazine. Reprinted with permission from Hu et al.[8] Copyright 2018 AAAS.

Ce(IV)-alkoxy complex. The reaction starts with the homolysis of Ce(IV)-alkoxy complex initiated by the ligand-to-metal charge transfer (LMCT) excitation to generate a high-energy electrophilic alkoxy radical and a reduced Ce(III) species. Then, through the important HAT activation process, the alkoxy radical readily abstracts an H atom from a C–H bond of alkane to form nucleophilic alkyl radical species, which further couples with amino, alkyl, or aryl groups from other molecules to from a relatively stable intermediate radical species. At last, single electron reduction of the intermediate radical species by the Ce(III) regenerates Ce(IV) and gives the final products after protonation, thus completing the overall reaction. The synergistic merger of HAT and LMCT catalysis in this system provided a promising strategy using abundant and inexpensive catalytic materials to realize efficient and diversified methane functionalizations under mild conditions. The H abstraction process of methane using HAT in this study accomplished the key C–H activation step and was inspiring to the other radical-like methane conversion processes with the formation of methyl radicals.

CONCLUSIONS AND OUTLOOK

In order to overcome the challenge of low temperature methane conversion, future efforts should consistently focus on solving two essential issues, i.e., C–H bond activation and product protection, which respectively determine the final activity and selectivity of methane conversion in potential reaction systems. First, a rationally designed catalyst with desired active sites for C–H activation is a precondition of efficient methane conversion. According to the mechanisms of C–H activation by oxygen or metal atoms summarized in Figure 2, excellent thermo-, electro- or photocatalysts should either have the ability to convert the oxidants (such as O_2, H_2O, and H_2O_2) into actively adsorbed oxygen species to initiate H abstraction from CH_4, or directly activate the C–H bond through formation of a M–C bond. For the thermocatalytic methane conversion, confined TM SACs and clusters are attractive catalysts for low temperature conversion. In particular, confined SACs with a high degree of coordination unsaturation could have strong interactions with both oxidants and methane to respectively promote oxidative intermediate or M–C formation and finally activate the C–H bond. For electrocatalytic methane conversion, electrocatalysts based on TiO_2 and SnO_2 may be promising because of their low C–H activation energy.[93] Moreover, any photocatalytic system that could generate $O^{\bullet -}$ (hole center), •OH, •O–R, and other electrophilic intermediates alike under photoexcitation can be potentially useful for methane conversion. Second, in the absence of product protection or separation during the reaction, it seems very hard to obtain high methane conversion along with high oxygenated products selectivity regardless of reaction systems. The success of methanol protection through the formation of methanol derivatives has been widely verified in both thermocatalysis (heterogeneous and homogeneous) and electrocatalysis. However, the strong acidic reaction medium impedes the industrialization of related reaction processes. As an alternative means of product protection by strong acid, synthesizing new chemicals in the reaction processes involving the methylation reaction using CH_4 as the reactant is also a meaningful research direction for efficient CH_4 conversion.[8] Another practical route to obtain high product selectivity along with appreciable methane conversion is to use the multicomponent catalysts with the function of product stabilization. Considering the fact that Mo- and Cu-based catalysts generally display high selectivity to oxygenated products and low tendency for methane overoxidation, they have been used to improve methanol selectivity of the single-component catalysts.[21,22,104] Successful examples include the use of Cu-promoted Pd-ZSM-5[21] and Fe-ZSM-5[22] to attain more optimized CH_4 conversion and methanol selectivity.

The hydroxyl radical-initiated methane oxidation process in photocatalytic or H_2O_2 containing systems enables efficient C–H bond activation. However, the oxidation process and product distribution become uncontrollable because of the unselective oxidation of hydroxyl radicals once they are released into the reaction solution. Therefore, proper catalysts that could controllably activate the oxidant or using flow-type reaction systems to control the oxidant feeding speed and residence time[97] should be considered in order to give more favorable conversion and selectivity. The flow-type reaction systems require excellent activity of the catalysts to ensure an appreciable one-pass conversion rate. Future studies are recommended to pay more attention to the methane oxidation process beyond the hydroxyl radical route. Although H_2O_2 is a clean oxidant, which only emits water in reaction, the higher cost of H_2O_2 than the reaction products and difficulty in product separation from a dilute reaction solution make related reaction systems uneconomical and hard to commercialize. A possible solution to this problem is to oxidize CH_4 with *in-situ*-formed H_2O_2 by coupling the H_2O_2 synthesis process with methane oxidation. This can be realized by feeding a gas mixture of H_2,O_2 and CH_4 in the presence of a suitable bi-functional catalyst in the thermocatalysis system[105,106] or oxidizing CH_4 with H_2O_2 produced by electro- or photocatalytic oxygen reduction.

Direct POM in gas phase systems is promising for commercialization as to direct use of industrial downstream. In comparison with this potential significance, however, the liquid-phase reaction system seems more technically feasible for POM, which can deliver better conversion and selectivity.[87] Indeed, methane conversion in liquid phase is very impressive, especially in the coexistence systems of single-site catalysts and H_2O_2, where H_2O_2 assisted the active site formation for C–H activation at low temperature. We can see that high CH_4 conversion and high oxygenated product yield are consistently demonstrated in the reaction conditions with low temperatures, high pressure, liquid phase, single-site catalysts, and H_2O_2 since both thermodynamics and kinetics issues are well resolved in these systems. Oxygen is the most ideal oxidant for environmental and economic reasons. At present, room-temperature direct methane conversion with oxygen is realized in many photocatalytic systems, while the thermocatalytic systems for this purpose are very scarce.[9] In this point, the design of efficient catalysts that can activate oxygen at low temperature is necessary. Again, in the future, important progresses would be expected in high pressure and liquid phase reaction systems.

Homogeneous methane conversion over molecular catalysts has the advantage of low reaction temperature. The confined TM SACs bridge the gap between homogeneous and heterogeneous catalysis and they can be relied upon in view of the high C–H bond dissociation rate. Therefore, it is possible to use confined SACs to realize efficient methane conversion at low temperature. The confined SACs on 2D materials with unique electronic states and their relationship with methane and oxygen activation should be of great interest.[107–110] Moreover, besides constructing active sites for oxygen activation to activate C–H through a radical-like mechanism, rational design of highly unsaturated single atom or single atom alloy catalysts for methane activation through the M–C σ-bond formation mechanism is also an important direction. Recently, Pt/Cu single-atom alloys have been proved to be able to efficiently activate the partial dehydrogenation of CH_4 without coke formation, overcoming the inability of Cu for efficient C–H activation and tendency of coke formation on Pt.[111]

Efforts are also needed in the aspect of accurate analysis of reaction products. The *in operando* TOF-MS is a powerful means to trace the product evolution in real time, and ^{13}C NMR is necessary to confirm the source of carbon-containing products. In combination with experimental characterizations and theoretical studies, the detailed reaction mechanism during methane oxidation could be revealed.[17] Beyond these aspects, it is feasible to couple multiple driving forces from thermal, electric, and solar energy and integrate the advantages of each approach in one reaction system to jointly break the tough structure of methane. In this case, developing multifunctional composite catalysts that can utilize thermal, electric, and photonic energy along with excellent C–H activation ability will have new opportunities for low-temperature methane conversion. If all the above-mentioned concerns can be fully considered, a more efficient, selective, and energy-efficient CH_4 conversion could be expected.

ACKNOWLEDGMENTS

We gratefully acknowledge the financial support from the Ministry of Science and Technology of China (nos. 2016YFA0204100 and 2016YFA0200200), the National Natural Science Foundation of China (nos. 21890753 and 21573220), the Key Research Program of Frontier Sciences of the Chinese Academy of Sciences (CAS) (no. QYZDB-SSW-JSC020), and the CAS DNL Cooperation Fund (no. DNL180201).

This work is dedicated to the 70th anniversary of the CAS Dalian Institute of Chemical Physics.

REFERENCES AND NOTES

1. Schwach, P., Pan, X., and Bao, X. (2017). Direct conversion of methane to value-added chemicals over heterogeneous catalysts: challenges and prospects. Chem. Rev. *117*, 8497–8520.
2. Guo, X., Fang, G., Li, G., Ma, H., Fan, H., Yu, L., Ma, C., Wu, X., Deng, D., Wei, M., et al. (2014). Direct, nonoxidative conversion of methane to ethylene, aromatics, and hydrogen. Science *344*, 616–619.
3. Tang, P., Zhu, Q., Wu, Z., and Ma, D. (2014). Methane activation: the past and future. Energy Environ. Sci. *7*, 2580–2591.
4. Adebajo, M.O. (2007). Green chemistry perspectives of methane conversion via oxidative methylation of aromatics over zeolite catalysts. Green Chem. *9*, 526.
5. Dou, Y., Pang, Y., Gu, L., Ding, Y., Jiang, W., Feng, X., Ji, W., and Au, C.-T. (2018). Core-shell structured Ru-Ni@SiO_2: active for partial oxidation of methane with tunable H_2/CO ratio. J. Energy Chem. *27*, 883–889.
6. German, E.D., and Sheintuch, M. (2013). Predicting CH_4 dissociation kinetics on metals: trends, sticking coefficients, H tunneling, and kinetic isotope effect. J. Phys. Chem. C *117*, 22811–22826.
7. Latimer, A.A., Kulkarni, A.R., Aljama, H., Montoya, J.H., Yoo, J.S., Tsai, C., Abild-Pedersen, F., Studt, F., and Nørskov, J.K. (2017). Understanding trends in C–H bond activation in heterogeneous catalysis. Nat. Mater. *16*, 225–229.
8. Hu, A., Guo, J.J., Pan, H., and Zuo, Z. (2018). Selective functionalization of methane, ethane, and higher alkanes by cerium photocatalysis. Science *361*, 668–672.
9. Liang, Z., Li, T., Kim, M., Asthagiri, A., and Weaver, J.F. (2017). Low-temperature activation of methane on the IrO_2(110) surface. Science *356*, 299–303.
10. Su, Y.Q., Liu, J.X., Filot, I.A.W., Zhang, L., and Hensen, E.J.M. (2018). Highly active and stable CH_4 oxidation by substitution of Ce^{4+} by two Pd^{2+} ions in CeO_2(111). ACS Catal. *8*, 6552–6559.
11. Shilov, A.E., and Shul'pin, G.B. (1997). Activation of C−H bonds by metal complexes. Chem. Rev. *97*, 2879–2932.
12. Conley, B.L., Tenn, W.J., Young, K.J.H., Ganesh, S.K., Meier, S.K., Ziatdinov, V.R., Mironov, O., Oxgaard, J., Gonzales, J., Goddard, W.A., et al. (2006). Design and study of homogeneous catalysts for the selective, low temperature oxidation of hydrocarbons. J. Mol. Catal. A *251*, 8–23.
13. Scapinello, M., Delikonstantis, E., and Stefanidis, G.D. (2017). The panorama of plasma-assisted non-oxidative methane reforming. Chem. Eng. Process. *117*, 120–140.
14. Agarwal, N., Freakley, S.J., McVicker, R.U., Althahban, S.M., Dimitratos, N., He, Q., Morgan, D.J., Jenkins, R.L., Willock, D.J., Taylor, S.H., et al. (2017). Aqueous Au-Pd colloids catalyze selective CH_4 oxidation to CH_3OH with O_2 under mild conditions. Science *358*, 223–227.
15. Zuo, Z., Ramírez, P.J., Senanayake, S.D., Liu, P., and Rodriguez, J.A. (2016). Low-temperature conversion of methane to methanol on CeO_x/Cu_2O catalysts: water controlled activation of the C–H bond. J. Am. Chem. Soc. *138*, 13810–13813.
16. Lustemberg, P.G., Palomino, R.M., Gutiérrez, R.A., Grinter, D.C., Vorokhta, M., Liu, Z., Ramírez, P.J., Matolín, V., Ganduglia-Pirovano, M.V., Senanayake, S.D., et al. (2018). Direct conversion of methane to methanol on Ni-ceria surfaces: metal–support interactions and water-enabled catalytic conversion by site blocking. J. Am. Chem. Soc. *140*, 7681–7687.
17. Cui, X., Li, H., Wang, Y., Hu, Y., Hua, L., Li, H., Han, X., Liu, Q., Yang, F., He, L., et al. (2018). Room-temperature methane conversion by graphene-confined single iron atoms. Chem *4*, 1902–1910.
18. Kwon, Y., Kim, T.Y., Kwon, G., Yi, J., and Lee, H. (2017). Selective activation of methane on single-atom catalyst of rhodium dispersed on zirconia for direct conversion. J. Am. Chem. Soc. *139*, 17694–17699.
19. Tang, Y., Li, Y., Fung, V., Jiang, D.E., Huang, W., Zhang, S., Iwasawa, Y., Sakata, T., Nguyen, L., Zhang, X., et al. (2018). Single rhodium atoms anchored in micropores for efficient transformation of methane under mild conditions. Nat. Commun. *9*, 1231.
20. Shan, J., Li, M., Allard, L.F., Lee, S., and Flytzani-Stephanopoulos, M. (2017). Mild oxidation of methane to methanol or acetic acid on supported isolated rhodium catalysts. Nature *551*, 605–608.
21. Huang, W., Zhang, S., Tang, Y., Li, Y., Nguyen, L., Li, Y., Shan, J., Xiao, D., Gagne, R., Frenkel, A.I., et al. (2016). Low-temperature transformation of methane to methanol on Pd_1O_4 single sites anchored on the internal surface of microporous silicate. Angew. Chem. Int. Ed. *55*, 13441–13445.
22. Hammond, C., Forde, M.M., Ab Rahim, M.H., Thetford, A., He, Q., Jenkins, R.L., Dimitratos, N., Lopez-Sanchez, J.A., Dummer, N.F., Murphy, D.M., et al. (2012). Direct catalytic conversion of methane to methanol in an aqueous medium by using copper-promoted Fe-ZSM-5. Angew. Chem. Int. Ed. *51*, 5129–5133.
23. Osadchii, D.Y., Olivos-Suarez, A.I., Szécsényi, Á., Li, G., Nasalevich, M.A., Dugulan, I.A., Crespo, P.S., Hensen, E.J.M., Veber, S.L., Fedin, M.V., et al. (2018). Isolated fe sites in metal organic frameworks catalyze the direct conversion of methane to methanol. ACS Catal. *8*, 5542–5548.
24. Ikuno, T., Zheng, J., Vjunov, A., Sanchez-Sanchez, M., Ortuño, M.A., Pahls, D.R., Fulton, J.L., Camaioni, D.M., Li, Z., Ray, D., et al. (2017). Methane oxidation to methanol catalyzed by Cu-oxo clusters stabilized in NU-1000 metal–organic framework. J. Am. Chem. Soc. *139*, 10294–10301.
25. Mironov, O.A., Bischof, S.M., Konnick, M.M., Hashiguchi, B.G., Ziatdinov, V.R., Goddard, W.A., III, Ahlquist, M., and Periana, R.A. (2013). Using reduced catalysts for oxidation reactions: mechanistic studies of the "periana-Catalytica" system for CH_4 oxidation. J. Am. Chem. Soc. *135*, 14644–14658.
26. Tomita, A., Nakajima, J., and Hibino, T. (2008). Direct oxidation of methane to methanol at low temperature and pressure in an electrochemical fuel cell. Angew. Chem. Int. Ed. *47*, 1462–1464.
27. Lee, B., and Hibino, T. (2011). Efficient and selective formation of methanol from methane in a fuel cell-type reactor. J. Catal. *279*, 233–240.
28. Spinner, N., and Mustain, W.E. (2013). Electrochemical methane activation and conversion to oxygenates at room temperature. J. Electrochem. Soc. *160*, F1275–F1281.
29. Rocha, R.S., Reis, R.M., Lanza, M.R.V., and Bertazzoli, R. (2013). Electrosynthesis of methanol from methane: the role of V_2O_5 in the reaction selectivity for methanol of a $TiO_2/RuO_2/V_2O_5$ gas diffusion electrode. Electrochim. Acta *87*, 606–610.
30. Li, W., He, D., Hu, G., Li, X., Banerjee, G., Li, J., Lee, S.H., Dong, Q., Gao, T., Brudvig, G.W., et al. (2018). Selective Co production by photoelectrochemical methane oxidation on TiO_2. ACS Cent. Sci. *4*, 631–637.
31. O'Reilly, M.E., Kim, R.S., Oh, S., and Surendranath, Y. (2017). Catalytic methane monofunctionalization by an electrogenerated high-valent Pd intermediate. ACS Cent. Sci. *3*, 1174–1179.
32. Yuliati, L., Itoh, H., and Yoshida, H. (2006). Preparation of isolated highly dispersed titanium oxides on silica by sol-gel method for photocatalytic non-oxidative direct methane coupling. Stud. Surf. Sci. Catal. *162*, 961–968.
33. Murcia-López, S., Villa, K., Andreu, T., and Morante, J.R. (2015). Improved selectivity for partial oxidation of methane to methanol in the presence of nitrite ions and $BiVO_4$ photocatalyst. Chem. Commun. *51*, 7249–7252.
34. Xie, J.J., Jin, R.X., Li, A., Bi, Y.P., Ruan, Q.S., Deng, Y.C., Zhang, Y.J., Yao, S.Y., Sankar, G., Ma, D., et al. (2018). Highly selective oxidation of methane to methanol at ambient conditions by titanium dioxide-supported iron species. Nat. Catal. *1*, 889–896.

35. Sastre, F., Fornés, V., Corma, A., and García, H. (2011). Selective, room-temperature transformation of methane to c1 oxygenates by deep UV photolysis over zeolites. J. Am. Chem. Soc. *133*, 17257–17261.

36. Li, L., Li, G.D., Yan, C., Mu, X.Y., Pan, X.L., Zou, X.X., Wang, K.X., and Chen, J.S. (2011). Efficient sunlight-driven dehydrogenative coupling of methane to ethane over a Zn^+-modified zeolite. Angew. Chem. Int. Ed. *50*, 8299–8303.

37. Ravi, M., Ranocchiari, M., and van Bokhoven, J.A. (2017). The direct catalytic oxidation of methane to methanol-a critical assessment. Angew. Chem. Int. Ed. *56*, 16464–16483.

38. Labinger, J.A., and Bercaw, J.E. (2002). Understanding and exploiting C-H bond activation. Nature *417*, 507–514.

39. Shilov, A.E., and Shulpin, G.B. (1987). Activation and Catalytic Reactions of Alkanes in Solutions of Metal-Complexes. Russian Chem. Rev. *56*, 754–792.

40. Periana, R.A., Taube, D.J., Gamble, S., Taube, H., Satoh, T., and Fujii, H. (1998). Platinum catalysts for the high-yield oxidation of methane to a methanol derivative. Science *280*, 560–564.

41. Cheng, J., Li, Z., Haught, M., and Tang, Y. (2006). Direct methane conversion to methanol by ionic liquid-dissolved platinum catalysts. Chem. Commun. *44*, 4617–4619.

42. Zimmermann, T., Soorholtz, M., Bilke, M., and Schüth, F. (2016). Selective methane oxidation catalyzed by platinum salts in oleum at turnover frequencies of large-scale industrial processes. J. Am. Chem. Soc. *138*, 12395–12400.

43. Periana, R.A., Taube, D.J., Evitt, E.R., Loffler, D.G., Wentrcek, P.R., Voss, G., and Masuda, T. (1993). A mercury-catalyzed, high-yield system for the oxidation of methane to methanol. Science *259*, 340–343.

44. Cundari, T.R., and Yoshikawa, A. (1998). Computational study of methane activation by mercury(II) complexes. J. Comput. Chem. *19*, 902–911.

45. Mukhopadhyay, S., and Bell, A.T. (2004). Catalyzed sulfonation of methane to methanesulfonic acid. J. Mol. Catal. A *211*, 59–65.

46. Sen, A., Benvenuto, M.A., Lin, M.R., Hutson, A.C., and Basickes, N. (1994). Activation of methane and ethane and their selective oxidation to the alcohols in protic media. J. Am. Chem. Soc. *116*, 998–1003.

47. Basickes, N., Hogan, T.E., and Sen, A. (1996). Radical-initiated functionalization of methane and ethane in fuming sulfuric acid. J. Am. Chem. Soc. *118*, 13111–13112.

48. Michalkiewicz, B., Kalucki, K., and Sosnicki, J.G. (2003). Catalytic system containing metallic palladium in the process of methane partial oxidation. J. Catal. *215*, 14–19.

49. Periana, R.A., Mironov, O., Taube, D., Bhalla, G., and Jones, C.J. (2003). Catalytic, oxidative condensation of CH_4 to CH_3COOH in one step via CH activation. Science *301*, 814–818.

50. Zerella, M., Mukhopadhyay, S., and Bell, A.T. (2004). Direct oxidation of methane to acetic acid catalyzed by Pd^{2+} and Cu^{2+} in the presence of molecular oxygen. Chem. Commun. *17*, 1948–1949.

51. Zerella, M., Kahros, A., and Bell, A.T. (2006). Methane oxidation to acetic acid catalyzed by Pd^{2+} cations in the presence of oxygen. J. Catal. *237*, 111–117.

52. An, Z., Pan, X., Liu, X., Han, X., and Bao, X. (2006). Combined redox couples for catalytic oxidation of methane by dioxygen at low temperatures. J. Am. Chem. Soc. *128*, 16028–16029.

53. Lin, M., and Sen, A. (1994). Direct catalytic conversion of methane to acetic acid in an aqueous medium. Nature *368*, 613–615.

54. Lin, M.R., Hogan, T.E., and Sen, A. (1996). Catalytic carbon-carbon and carbon-hydrogen bond cleavage in lower alkanes. Low-temperature hydroxylations and hydroxycarbonylations with dioxygen as the oxidant. J. Am. Chem. Soc. *118*, 4574–4580.

55. Chepaikin, E.G., Boyko, G.N., Bezruchenko, A.P., Leshcheva, A.A., and Grigoryan, E.H. (1998). Oxidative carbonylation of methane in the presence of rh complexes in aqueous acetic acid. J. Mol. Catal. A *129*, 15–18.

56. Chepaikin, E.G., Bezruchenko, A.P., Leshcheva, A.A., Boyko, G.N., Kuzmenkov, I.V., Grigoryan, E.H., and Shilov, A.E. (2001). Functionalisation of methane under dioxygen and carbon monoxide catalyzed by rhodium complexes - oxidation and oxidative carbonylation. J. Mol. Catal. A *169*, 89–98.

57. Gunsalus, N.J., Koppaka, A., Park, S.H., Bischof, S.M., Hashiguchi, B.G., and Periana, R.A. (2017). Homogeneous functionalization of methane. Chem. Rev. *117*, 8521–8573.

58. Khan, M.M., and Somorjai, G.A. (1985). A kinetic-study of partial oxidation of methane with nitrous oxide on a molybdena-silica catalyst. J. Catal. *91*, 263–271.

59. Zhen, K. (1985). Partial oxidation of methane with nitrous oxide over V_2O_5-SiO_2 catalyst. J. Catal. *94*, 501–507.

60. Li, T., Wang, S.J., Yu, C.S., Ma, Y.C., Li, K.L., and Lin, L.W. (2011). Direct conversion of methane to methanol over nano-[Au/SiO_2] in [Bmim]Cl ionic liquid. Appl. Catal. A *398*, 150–154.

61. Tomkins, P., Ranocchiari, M., and van Bokhoven, J.A. (2017). Direct conversion of methane to methanol under mild conditions over Cu-zeolites and beyond. Acc. Chem. Res. *50*, 418–425.

62. Olivos-Suarez, A.I., Szécsényi, À., Hensen, E.J.M., Ruiz-Martinez, J., Pidko, E.A., and Gascon, J. (2016). Strategies for the direct catalytic valorization of methane using heterogeneous catalysis: challenges and opportunities. ACS Catal. *6*, 2965–2981.

63. Smeets, P.J., Groothaert, M.H., and Schoonheydt, R.A. (2005). Cu based zeolites: a UV-vis study of the active site in the selective methane oxidation at low temperatures. Catal. Today *110*, 303–309.

64. Grundner, S., Markovits, M.A.C., Li, G., Tromp, M., Pidko, E.A., Hensen, E.J.M., Jentys, A., Sanchez-Sanchez, M., and Lercher, J.A. (2015). Single-site trinuclear copper oxygen clusters in mordenite for selective conversion of methane to methanol. Nat. Commun. *6*, 7546.

65. Pappas, D.K., Borfecchia, E., Dyballa, M., Pankin, I.A., Lomachenko, K.A., Martini, A., Signorile, M., Teketel, S., Arstad, B., Berlier, G., et al. (2017). Methane to methanol: structure–activity relationships for Cu-CHA. J. Am. Chem. Soc. *139*, 14961–14975.

66. Tomkins, P., Mansouri, A., Bozbag, S.E., Krumeich, F., Park, M.B., Alayon, E.M.C., Ranocchiari, M., and van Bokhoven, J.A. (2016). Isothermal cyclic conversion of methane into methanol over copper-exchanged zeolite at low temperature. Angew. Chem. Int. Ed. *55*, 5467–5471.

67. Sushkevich, V.L., Palagin, D., Ranocchiari, M., and van Bokhoven, J.A. (2017). Selective anaerobic oxidation of methane enables direct synthesis of methanol. Science *356*, 523–527.

68. Kim, Y., Kim, T.Y., Lee, H., and Yi, J. (2017). Distinct activation of Cu-MOR for direct oxidation of methane to methanol. Chem. Commun. *53*, 4116–4119.

69. Groothaert, M.H., Smeets, P.J., Sels, B.F., Jacobs, P.A., and Schoonheydt, R.A. (2005). Selective oxidation of methane by the bis(μ-oxo)dicopper core stabilized on ZSM-5 and mordenite zeolites. J. Am. Chem. Soc. *127*, 1394–1395.

70. Starokon, E.V., Parfenov, M.V., Pirutko, L.V., Abornev, S.I., and Panov, G.I. (2011). Room-temperature oxidation of methane by α-oxygen and extraction of products from the FeZSM-5 surface. J. Phys. Chem. C *115*, 2155–2161.

71. Wulfers, M.J., Teketel, S., Ipek, B., and Lobo, R.F. (2015). Conversion of methane to methanol on copper-containing small-pore zeolites and zeotypes. Chem. Commun. *51*, 4447–4450.

72. Narsimhan, K., Iyoki, K., Dinh, K., and Román-Leshkov, Y. (2016). Catalytic oxidation of methane into methanol over copper-exchanged zeolites with oxygen at low temperature. ACS Cent. Sci. *2*, 424–429.

73. Khan, N.A., Kennedy, E.M., Dlugogorski, B.Z., Adesina, A.A., and Stockenhuber, M. (2017). Reaction of nitrous oxide with methane to synthesis gas: a thermodynamic and catalytic study. J. Energy Chem. *26*, 155–162.

74. Chow, Y.K., Dummer, N.F., Carter, J.H., Meyer, R.J., Armstrong, R.D., Williams, C., Shaw, G., Yacob, S., Bhasin, M.M., Willock, D.J., et al. (2018). A kinetic study of methane partial oxidation over Fe-ZSM-5 using N_2O as an oxidant. ChemPhysChem *19*, 402–411.

75. Sushkevich, V.L., Palagin, D., and van Bokhoven, J.A. (2018). The effect of the active-site structure on the activity of copper mordenite in the aerobic and anaerobic conversion of methane into methanol. Angew. Chem. Int. Ed. Engl. *57*, 8906–8910.

76. Al-Shihri, S., Richard, C.J., and Chadwick, D. (2017). Selective oxidation of methane to

methanol over ZSM-5 catalysts in aqueous hydrogen peroxide: role of formaldehyde. ChemCatChem *9*, 1276–1283.

77. Narsimhan, K., Michaelis, V.K., Mathies, G., Gunther, W.R., Griffin, R.G., and Román-Leshkov, Y. (2015). Methane to acetic acid over cu-exchanged zeolites: mechanistic insights from a site-specific carbonylation reaction. J. Am. Chem. Soc. *137*, 1825–1832.

78. Wu, J.F., Yu, S.M., Wang, W.D., Fan, Y.X., Bai, S., Zhang, C.W., Gao, Q., Huang, J., and Wang, W. (2013). Mechanistic insight into the formation of acetic acid from the direct conversion of methane and carbon dioxide on zinc-modified H-ZSM-5 zeolite. J. Am. Chem. Soc. *135*, 13567–13573.

79. Rabie, A.M., Betiha, M.A., and Park, S.-E. (2017). Direct synthesis of acetic acid by simultaneous co-activation of methane and CO_2 over cu-exchanged ZSM-5 catalysts. Appl. Catal. B *215*, 50–59.

80. Sirijaraensre, J., and Limtrakul, J. (2015). Modification of the catalytic properties of the Au_4 nanocluster for the conversion of methane-to-methanol: synergistic effects of metallic adatoms and a defective graphene support. Phys. Chem. Chem. Phys. *17*, 9706–9715.

81. Yuan, J.Y., Zhang, W.H., Li, X.X., and Yang, J.L. (2018). A high performance catalyst for methane conversion to methanol: graphene supported single atom Co. Chem. Commun. *54*, 2284–2287.

82. Wu, S.Y., Lin, C.H., and Ho, J.J. (2015). Density-functional calculations of the conversion of methane to methanol on platinum-decorated sheets of graphene oxide. Phys. Chem. Chem. Phys. *17*, 26191–26197.

83. Latimer, A.A., Aljama, H., Kakekhani, A., Yoo, J.S., Kulkarni, A., Tsai, C., Garcia-Melchor, M., Abild-Pedersen, F., and Nørskov, J.K. (2017). Mechanistic insights into heterogeneous methane activation. Phys. Chem. Chem. Phys. *19*, 3575–3581.

84. Wang, Y. (2018). Room-temperature conversion of methane becomes true. Joule *2*, 1399–1401.

85. Deng, D., Chen, X., Yu, L., Wu, X., Liu, Q., Liu, Y., Yang, H., Tian, H., Hu, Y., Du, P., et al. (2015). A single iron site confined in a graphene matrix for the catalytic oxidation of benzene at room temperature. Sci. Adv. *1*, e1500462.

86. Palkovits, R., Antonietti, M., Kuhn, P., Thomas, A., and Schuth, F. (2009). Solid catalysts for the selective low-temperature oxidation of methane to methanol. Angew. Chem. Int. Ed. *48*, 6909–6912.

87. Latimer, A.A., Kakekhani, A., Kulkarni, A.R., and Nørskov, J.K. (2018). Direct methane to methanol: the selectivity–conversion limit and design strategies. ACS Catal. *8*, 6894–6907.

88. Xie, S., Lin, S., Zhang, Q., Tian, Z., and Wang, Y. (2018). Selective electrocatalytic conversion of methane to fuels and chemicals. J. Energy Chem. *27*, 1629–1636.

89. Jirkovský, J.S., Panas, I., Ahlberg, E., Halasa, M., Romani, S., and Schiffrin, D.J. (2011). Single atom hot-spots at Au–Pd nanoalloys for electrocatalytic H_2O_2 production. J. Am. Chem. Soc. *133*, 19432–19441.

90. Rankin, R.B., and Greeley, J. (2012). Trends in selective hydrogen peroxide production on transition metal surfaces from first principles. ACS Catal. *2*, 2664–2672.

91. Edwards, J.K., Solsona, B., N, E.N., Carley, A.F., Herzing, A.A., Kiely, C.J., and Hutchings, G.J. (2009). Switching off hydrogen peroxide hydrogenation in the direct synthesis process. Science *323*, 1037–1041.

92. Lee, B., Sakamoto, Y., Hirabayashi, D., Suzuki, K., and Hibino, T. (2010). Direct oxidation of methane to methanol over proton conductor/metal mixed catalysts. J. Catal. *271*, 195–200.

93. Arnarson, L., Schmidt, P.S., Pandey, M., Bagger, A., Thygesen, K.S., Stephens, I.E.L., and Rossmeisl, J. (2018). Fundamental limitation of electrocatalytic methane conversion to methanol. Phys. Chem. Chem. Phys. *20*, 11152–11159.

94. Yuliati, L., and Yoshida, H. (2008). Photocatalytic conversion of methane. Chem. Soc. Rev. *37*, 1592–1602.

95. Murcia-López, S., Villa, K., Andreu, T., and Morante, J.R. (2014). Partial oxidation of methane to methanol using bismuth-based photocatalysts. ACS Catal. *4*, 3013–3019.

96. Murcia-López, S., Bacariza, M.C., Villa, K., Lopes, J.M., Henriques, C., Morante, J.R., and Andreu, T. (2017). Controlled photocatalytic oxidation of methane to methanol through surface modification of beta zeolites. ACS Catal. *7*, 2878–2885.

97. López-Martín, Á., Caballero, A., and Colón, G. (2017). Photochemical methane partial oxidation to methanol assisted by H_2O_2. J. Photochem. Photobiol. A *349*, 216–223.

98. Meng, X., Liu, L., Ouyang, S., Xu, H., Wang, D., Zhao, N., and Ye, J. (2016). Nanometals for solar-to-chemical energy conversion: from semiconductor-based photocatalysis to plasmon-mediated photocatalysis and photo-thermocatalysis. Adv. Mater. *28*, 6781–6803.

99. Liu, H., Meng, X., Dao, T.D., Zhang, H., Li, P., Chang, K., Wang, T., Li, M., Nagao, T., and Ye, J. (2015). Conversion of carbon dioxide by methane reforming under visible-light irradiation: surface-plasmon-mediated nonpolar molecule activation. Angew. Chem. Int. Ed. Engl. *54*, 11545–11549.

100. Song, H., Meng, X., Wang, Z.-j., Wang, Z., Chen, H., Weng, Y., Ichihara, F., Oshikiri, M., Kako, T., and Ye, J. (2018). Visible-light-mediated methane activation for steam methane reforming under mild conditions: a case study of Rh/TiO_2 catalysts. ACS Catal. *8*, 7556–7565.

101. Sanz, J.M., Ortiz, D., Alcaraz de la Osa, R., Saiz, J.M., González, F., Brown, A.S., Losurdo, M., Everitt, H.O., and Moreno, F. (2013). UV plasmonic behavior of various metal nanoparticles in the near- and far-field regimes: geometry and substrate effects. J. Phys. Chem. C *117*, 19606–19615.

102. Song, H., Meng, X., Dao, T.D., Zhou, W., Liu, H., Shi, L., Zhang, H., Nagao, T., Kako, T., and Ye, J. (2018). Light-enhanced carbon dioxide activation and conversion by effective plasmonic coupling effect of Pt and Au nanoparticles. ACS Appl. Mater. Interfaces *10*, 408–416.

103. Liu, H., Meng, X., Dao, T.D., Liu, L., Li, P., Zhao, G., Nagao, T., Yang, L., and Ye, J. (2017). Light assisted CO_2 reduction with methane over SiO_2 encapsulated Ni nanocatalysts for boosted activity and stability. J. Mater. Chem. A *5*, 10567–10573.

104. Zhang, X., He, D., Zhang, Q., Xu, B., and Zhu, Q. (2005). Comparative studies on direct conversion of methane to methanol/formaldehyde over La–Co–O and ZrO_2 supported molybdenum oxide catalysts. Top. Catal. *32*, 215–223.

105. Freakley, S.J., He, Q., Harrhy, J.H., Lu, L., Crole, D.A., Morgan, D.J., Ntainjua, E.N., Edwards, J.K., Carley, A.F., Borisevich, A.Y., et al. (2016). Palladium-tin catalysts for the direct synthesis of H_2O_2 with high selectivity. Science *351*, 965–968.

106. Ab Rahim, M.H., Forde, M.M., Jenkins, R.L., Hammond, C., He, Q., Dimitratos, N., Lopez-Sanchez, J.A., Carley, A.F., Taylor, S.H., Willock, D.J., et al. (2013). Oxidation of methane to methanol with hydrogen peroxide using supported gold-palladium alloy nanoparticles. Angew. Chem. Int. Ed. *52*, 1280–1284.

107. Deng, D., Novoselov, K.S., Fu, Q., Zheng, N., Tian, Z., and Bao, X. (2016). Catalysis with two-dimensional materials and their heterostructures. Nat. Nanotechnol. *11*, 218–230.

108. Wang, Y., Mao, J., Meng, X., Yu, L., Deng, D., and Bao, X. (2019). Catalysis with two-dimensional materials confining single atoms: concept, design, and applications. Chem. Rev. *119*, 1806–1854.

109. Chen, X., Yu, L., Wang, S., Deng, D., and Bao, X. (2017). Highly active and stable single iron site confined in graphene nanosheets for oxygen reduction reaction. Nano Energy *32*, 353–358.

110. Cui, X., Xiao, J., Wu, Y., Du, P., Si, R., Yang, H., Tian, H., Li, J., Zhang, W.-H., Deng, D., et al. (2016). A graphene composite material with single cobalt active sites: a highly efficient counter electrode for dye-sensitized solar cells. Angew. Chem. Int. Ed. *55*, 6708–6712.

111. Marcinkowski, M.D., Darby, M.T., Liu, J., Wimble, J.M., Lucci, F.R., Lee, S., Michaelides, A., Flytzani-Stephanopoulos, M., Stamatakis, M., and Sykes, E.C.H. (2018). Pt/Cu single-atom alloys as coke-resistant catalysts for efficient C–H activation. Nat. Chem. *10*, 325–332.